# Asymmetric Spike Patterns for the One-Dimensional Gierer-Meinhardt Model: Equilibria and Stability

Michael J. Ward [1], Juncheng Wei[2]

**Abstract**

Equilibrium solutions to the one-dimensional Gierer-Meinhardt model in the form of sequences of spikes of different heights are constructed asymptotically in the limit of small activator diffusivity $\varepsilon$. For a pattern with $k$ spikes, the construction yields $k_1$ spikes that have a common small amplitude and $k_2 = k - k_1$ spikes that have a common large amplitude. A $k$-spike asymmetric equilibrium solution is obtained from an arbitrary ordering of the small and large spikes on the domain. It is shown that such solutions exist when the inhibitor diffusivity $D$ is less than some critical value $D_m$ that depends on $k_1$, on $k_2$, and on other parameters associated with the Gierer-Meinhardt model. It is also shown that these asymmetric $k$-spike solutions bifurcate from the symmetric solution branch $s_k$, for which $k$ spikes have equal height. These asymmetric solutions provide connections between the branch $s_k$ and the other symmetric branches $s_j$, for $j = 1, .., k-1$. The stability of the asymmetric $k$-spike patterns with respect to the large $O(1)$ eigenvalues and the small $O(\varepsilon^2)$ eigenvalues is also analyzed. It is found that the asymmetric patterns are stable with respect to the large $O(1)$ eigenvalues when $D > D_e$, where $D_e$ depends on $k_1$ and $k_2$, on certain parameters in the model, and on the specific ordering of the small and large spikes within a given $k$-spike sequence. Numerical values for $D_e$ are obtained from numerical solutions of a matrix eigenvalue problem. Another matrix eigenvalue problem that determines the small eigenvalues is derived. For the examples considered, it is shown that the bifurcating asymmetric branches are all unstable with respect to these small eigenvalues.

## 1 Introduction

Turing [12] proposed that localized peaks in the concentration of a chemical substance, known as a morphogen, could be responsible for the process of morphogenesis, which describes the development of a complex organism from a single cell. Through the use of a linearized analysis, he showed how stable spatially complex patterns can develop from small perturbations of spatially homogeneous initial data for a coupled system of reaction-diffusion equations. Since Turing's paper, many reaction-diffusion models have been proposed for pattern formation, including the well-known activator-inhibitor model postulated by Gierer and Meinhardt [3]. They showed numerically that their model, referred to here as the GM model, can produce a highly localized pattern for the activator concentration. There has been much subsequent numerical work on classifying pattern

[1]Department of Mathematics, University of British Columbia, Vancouver, Canada V6T 1Z2
[2]Department of Mathematics, Chinese University of Hong Kong, Shatin, New Territories, Hong Kong

formation aspects of this model, including the development of spikes and stripes (cf. [4], [8] and the references therein).

In recent years there has been a considerable effort to analyze the existence, stability, and dynamics of localized solutions to the singularly perturbed GM model, in which the activator diffuses much more slowly than does the inhibitor. One of the goals of this type of analysis is to asymptotically construct equilibrium solutions in the form of spikes in the activator concentration and to determine the locations of these spikes. A second main focus is to determine the conditions on the parameters that ensure the linear stability of these types of solutions. It is important to emphasize that this type of stability analysis is very different from the classical Turing-type stability analysis based on linearizing a reaction-diffusion system around a spatially homogeneous steady-state equilibrium solution. The stability analysis, for perturbations of localized solutions, typically leads to singularly perturbed eigenvalue problems with spatially inhomogeneous coefficients that are difficult to study analytically. A mathematical survey of results on spike solutions to the GM model is given in [9] and [14].

The goal of this paper is to determine conditions for the existence and linear stability of certain *asymmetric* equilibrium spike patterns for the following simplified form of the singularly perturbed one-dimensional GM model:

$$a_t = \varepsilon^2 a_{xx} - a + \frac{a^p}{h^q}\,, \qquad -1 < x < 1\,, \quad t > 0\,, \tag{1.1a}$$

$$0 = D h_{xx} - \mu h + \varepsilon^{-1}\frac{a^m}{h^s}\,, \qquad -1 < x < 1\,, \quad t > 0\,, \tag{1.1b}$$

$$a_x(\pm 1, t) = h_x(\pm 1, t) = 0\,. \tag{1.1c}$$

Here $a$, $h$, $\varepsilon \ll 1$, $D > 0$, and $\mu > 0$ represent the scaled activator concentration, inhibitor concentration, small activator diffusivity, inhibitor diffusivity, and constant inhibitor decay rate. The exponents $(p, q, m, s)$ in (1.1) are assumed to satisfy

$$p > 1, \qquad q > 0, \qquad m > 0, \qquad s \geq 0, \qquad 0 < \frac{p-1}{q} < \frac{m}{s+1}\,. \tag{1.2}$$

The dimensional analysis leading to (1.1) is given in [6]. The simplification to the GM model that is made is that we neglect the time derivative of the inhibitor field.

The asymmetric equilibrium solutions to (1.1) that we construct in the limit $\varepsilon \to 0$ have the form of a sequence of spikes of different heights. Specifically, for a pattern with $k$ spikes, our asymptotic construction yields $k_1 > 0$ spikes that have a common small amplitude and $k_2 = k - k_1 > 0$ spikes that have a common large amplitude. A $k$-spike asymmetric equilibrium solution is obtained from

an arbitrary ordering of the small and large spikes across the interval. The idea that such patterns should exist was communicated to us by Doelman [2]. An example of such a spike pattern that is obtained from the analysis is shown in Fig. 1. We show that such solutions exist when $D$ is less than some critical value $D_m$ that depends on $k_1$, $k_2$, $\mu$, and $r \equiv (p-1)/[qm-(p-1)(s+1)]$. Further, more refined results, including the possibility of multiplicity of asymmetric spike patterns for a specific set of the parameters with the same ordering of the spikes, are also obtained. The equilibrium results are given in Proposition 2.1. By plotting a bifurcation diagram of a norm of $a$ versus $D$, we show that the $k$-spike asymmetric solutions bifurcate from the symmetric branch $s_k$ for which $k$ spikes have an equal amplitude. Specifically, we show that the $k$-spike asymmetric branch with $k_1$ small spikes provides the connection as $D$ is varied between the symmetric branches $s_k$ and $s_{k-k_1}$. The asymptotic analysis leading to these results is based on a formal application of the method of matched asymptotic expansions. To our knowledge this is the first time that asymmetric equilibrium spike patterns have been demonstrated for the GM model.

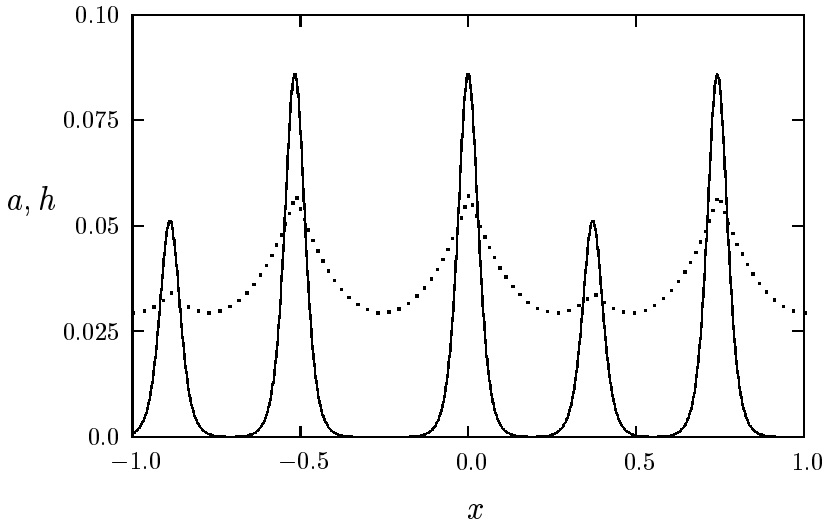


Figure 1: Plot of the activator and inhibitor concentration for a five-spike asymptotic asymmetric equilibrium solution with $\epsilon = .02$, $D = .04$, $\mu = 1$, and $(p, q, m, s) = (2, 1, 2, 0)$. The solid curve is the activator concentration and the dotted curve is the inhibitor concentration.

Next, we analyze the linear stability of these asymmetric equilibrium spike patterns. There are two classes of eigenvalues to be considered: the large $O(1)$ eigenvalues and the small $O(\varepsilon^2)$ eigenvalues. For the large eigenvalues, we obtain an explicit stability criterion for the asymmetric

spike patterns in terms of the maximum eigenvalue of a certain matrix eigenvalue problem. The result is given below in Proposition 3.1 and Corollary 3.1 and 3.2. We show that, with respect to the large $O(1)$ eigenvalues, the asymmetric spike solutions are stable when $D > D_e$, where the critical value $D_e$ depends on $k_1$, $k_2$, $\mu$, $r$, and on the specific orientation of the small and large spikes within a given $k$-spike sequence. When $r = 1$, which holds for the usual GM parameter set $(p, q, m, s) = (2, 1, 2, 0)$, we give an explicit formula below for $D_e$ in Result 4.1 for the two-spike case. For solutions with more than two spikes, numerical values for $D_e$ are obtained from a numerical calculation of the maximum eigenvalue of the matrix eigenvalue problem. The stability of the $k$-spike patterns with respect to the small eigenvalues of order $O(\varepsilon^2)$ is also studied. We derive a generalized matrix eigenvalue problem that determines the small eigenvalues. The result is given in Proposition 5.2. The value zero is a small eigenvalue of algebraic multiplicity $k-1$ at the value of $D$ for which the asymmetric $k$-spike patterns bifurcate from the symmetric branch $s_k$. From numerical computations of the generalized matrix eigenvalue problem in Proposition 5.2, we show that these bifurcating asymmetric branches are all unstable with respect to the small eigenvalues. Although all of these asymmetric patterns are ultimately unstable, our conclusions do indicate that there are ranges of $D$ for which asymmetric equilibria will persist for long time intervals of the order $t << O(\varepsilon^{-2})$. We remark that a somewhat similar approach to the stability of localized patterns was adopted in [10] for the Fitzhugh-Nagumo model.

The work in this paper is complementary to the study in [5] of the stability of spike patterns for (1.1) with spikes of equal height. These *symmetric* spike solutions can be constructed asymptotically for arbitrary values of $D$, and their existence was previously rigorously proved in [11] in the limit $\varepsilon \to 0$. It was shown in [5] that a symmetric $k$-spike solution with $k > 1$ will be linearly stable with respect to the large $O(1)$ eigenvalues when $D < D_k$. An explicit formula for $D_k$ was derived analytically in [5] in terms of $k$ and the exponents $(p, q, m, s)$. It was found that $D_k \to 0$ as $k \to \infty$. It was also shown in [5] that the symmetric $k$-spike solution will be stable with respect to the small $O(\varepsilon^2)$ eigenvalues when $D < D_k^*$, for some explicit values $D_k^*$ satisfying $D_k^* < D_k$. Thus, a $k$-spike symmetric pattern is stable with respect to both the large and small eigenvalues when $D < D_k^*$. In this paper we show that these critical values $D_k^*$ are precisely the values of $D$ at which asymmetric $k$-spike patterns bifurcate from the symmetric branch $s_k$.

The outline of this paper is as follows. In §2 we use the method of matched asymptotic expansions to construct a $k$-spike asymmetric equilibrium spike solution to (1.1). In §3 we determine conditions that ensure that the large $O(1)$ eigenvalues associated with the linearization of (1.1) about the asymmetric equilibrium solution have negative real parts. When this condition holds, we say that the pattern is stable with respect to the large $O(1)$ eigenvalues. Examples of the theory

for solutions with fewer than five spikes, together with some specific results for these solutions, are given in §4. In §5 we analyze the small eigenvalues and we calculate their algebraic sign numerically for the specific examples discussed in §4. Some concluding remarks are made in §6.

## 2 Asymmetric Equilibrium Solutions

For $\varepsilon \to 0$, we construct a $k$-spike asymmetric equilibrium solution to (1.1) in the form of a sequence of spikes of different heights.

To determine how spikes of different heights can arise, we first construct a symmetric one-spike equilibrium solution to (1.1) on a finite domain of length $2l$, where $l > 0$ is a parameter. The problem then is to find a solution to

$$\varepsilon^2 a_{xx} - a + \frac{a^p}{h^q} = 0\,, \qquad -l < x < l\,, \tag{2.1a}$$

$$Dh_{xx} - \mu h + \varepsilon^{-1}\frac{a^m}{h^s} = 0\,, \qquad -l < x < l\,, \tag{2.1b}$$

$$a_x(\pm l) = h_x(\pm l) = 0\,, \tag{2.1c}$$

which has exactly one spike centered at the origin. In the limit $\varepsilon \to 0$, such a solution has the property that $a$ and $h$ are even, that $a(l)$ is exponentially small, and that $h(l) = O(1)$. We would like to find all different values of $l$, labeled by $l_1$,..,$l_n$, such that $h(l_1) =, .., = h(l_n)$. For a certain range of the parameters, as obtained below, there are exactly two such values of $l$. These "local" solutions are then used to obtain a global asymmetric pattern for (1.1) on $[-1, 1]$.

The asymptotic solution to (2.1) proceeds in a similar way as in [5]. We obtain that

$$a(x) \sim [h(0)]^{\gamma}\, u_c(x/\varepsilon)\,, \qquad \text{where} \qquad \gamma = q/(p-1)\,, \tag{2.2}$$

and $u_c(y)$ is the unique solution to

$$u_c'' - u_c + u_c^p = 0\,, \qquad -\infty < y < \infty\,, \tag{2.3a}$$

$$u_c \to 0 \quad \text{as} \quad |y| \to \infty\,; \qquad u_c'(0) = 0\,, \qquad u_c(0) > 0\,. \tag{2.3b}$$

In particular, when $p = 2$ we have

$$u_c(y) = \frac{3}{2}\mathrm{sech}^2\,(y/2)\ . \tag{2.4}$$

Since $a$ is localized near $x = 0$, the term $\varepsilon^{-1}a^m/h^s$ in (2.1b) can be asymptotically approximated as a Dirac mass. Thus, when $\varepsilon \ll 1$, the problem for $h(x)$ is

$$Dh'' - \mu h = -[h(0)]^{\gamma m - s} \int_{-\infty}^{\infty} [u_c(y)]^m \, dy \; \delta(x) \,, \qquad -l < x < l \,, \tag{2.5a}$$

$$h'(\pm l) = 0 \,, \tag{2.5b}$$

where $\delta(x)$ is the delta function. The solution to (2.5) is

$$h(x) = [h(0)]^{\gamma m - s} \int_{-\infty}^{\infty} [u_c(y)]^m \, dy \; G_l(x;0) \,, \tag{2.6}$$

where $G_l(x;0)$ is the Green's function satisfying

$$DG_{lxx} - \mu G_l = -\delta(x) \,, \qquad -l < x < l \,, \tag{2.7a}$$

$$G_{lx}(\pm l;0) = 0 \,. \tag{2.7b}$$

A simple calculation gives,

$$G_l(x;0) = \frac{\cosh\left[(l - |x|)\sqrt{\mu/D}\right]}{2\sqrt{\mu D}\sinh\left(l\sqrt{\mu/D}\right)} \,. \tag{2.8}$$

Next, we readily calculate from (2.6) that $h(0)$ satisfies

$$[h(0)]^{\gamma m - (s+1)} = \left[ G_l(0;0) \int_{-\infty}^{\infty} [u_c(y)]^m \, dy \right]^{-1} \,, \tag{2.9}$$

for $i = 1, ..n$. In terms of $h(0)$, we can write $h(l)$ as

$$h(l) = h(0) \frac{G_l(l;0)}{G_l(0;0)} \,. \tag{2.10}$$

Finally, substituting (2.8) and (2.9) into (2.10), we obtain an explicit formula for $h(l)$ given by

$$h(l) = \left( \frac{2\sqrt{\mu D}}{\int_{-\infty}^{\infty} [u_c(y)]^m \, dy} \right)^r b\left[ l\sqrt{\mu/D} \right] \,. \tag{2.11}$$

Here the exponent $r$ and the function $b(z)$, for $z > 0$, are defined by

$$b(z) \equiv \frac{\tanh^r z}{\cosh z} \,, \qquad r \equiv \frac{1}{\gamma m - (s+1)} \,, \tag{2.12}$$

where $\gamma$ was defined in (2.2). From (1.2), we find that $r > 0$. The conditions for the existence and stability of asymmetric solutions will depend on $r$. Two common exponent parameter sets for the GM model and their values of $r$ are

$$\text{(i)} \quad (p, q, m, s) = (2, 1, 2, 0) \qquad r = 1\,; \qquad \text{(ii)} \quad (p, q, m, s) = (4, 2, 2, 0) \qquad r = 3\,. \tag{2.13}$$

The function $b(z) > 0$ in (2.12) has several key properties. It has a unique global maximum point at $z = z_c$, where

$$z_c = \log\left(\sqrt{r} + \sqrt{r+1}\right)\,. \tag{2.14}$$

In addition, it satisfies $b'(z) > 0$ on $[0, z_c)$ and $b'(z) < 0$ on $(z_c, \infty)$. Plots of $b(z)$ when $r = 1$ and when $r = 3$ are shown in Fig. 2(a) and Fig. 2(b), respectively. From the behavior of $b(z)$ we readily deduce the following result:

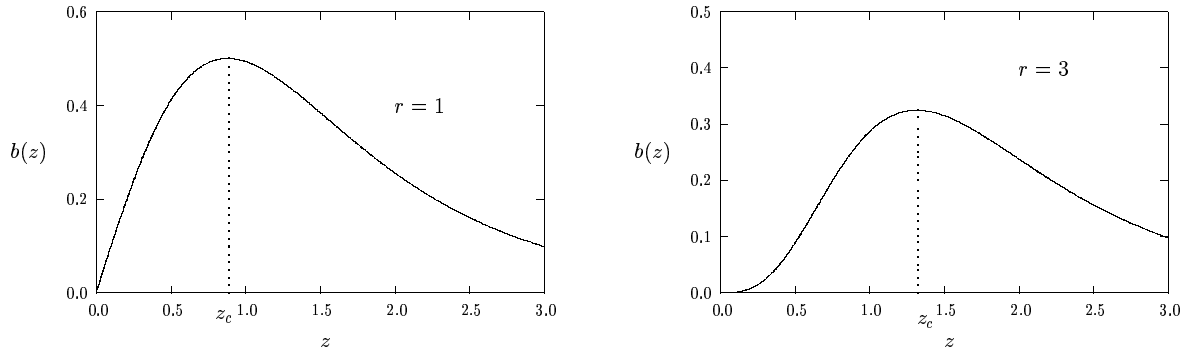


(a) $b(z)$ for $r = 1$

(b) $b(z)$ for $r = 3$

Figure 2: Plots of the function $b(z)$ versus $z$ for $r = 1$ and $r = 3$.

**Result 2.1**: *Let $r > 0$. For any $z \in (0, z_c)$, there exists a unique point $\tilde{z} = f(z)$, such that $\tilde{z} > z_c$, with the property that*

$$b(z) = b(\tilde{z}) \equiv b\left[f(z)\right]\,. \tag{2.15}$$

The implication of this result is the following:

**Result 2.2**: *Let $r > 0$. Given any $l$ with $l\sqrt{\mu/D} < z_c$, there exists a unique $\tilde{l}$, with $\tilde{l}\sqrt{\mu/D} \equiv \tilde{z} > z_c$, such that $h(l) = h(\tilde{l})$.*

Below, we need certain properties of the inverse function $f(z)$ defined in (2.15). For an arbitrary value of $r > 0$, $f(z)$ is convex on $(0, z_c)$, $f'(z) < -1$ on $(0, z_c)$, and $f'(z_c) = -1$. In general, $f(z)$ can only be obtained numerically. However, for the special case $r = 1$, we can calculate $f(z)$ analytically. Using (2.12) with $r = 1$ we get

$$\sinh z \sinh \tilde{z} = 1 \,. \tag{2.16}$$

Therefore,

$$\tilde{z} = f(z) \equiv \log\left[\mathrm{csch} z + \coth z\right] \,, \qquad \text{for} \quad z \in [0, z_c) \,. \tag{2.17}$$

A plot of $f(z)$ for the values $r = 1$ and $r = 3$, the latter obtained using Newton's method, is shown in Fig. 3(a) and Fig. 3(b), respectively.

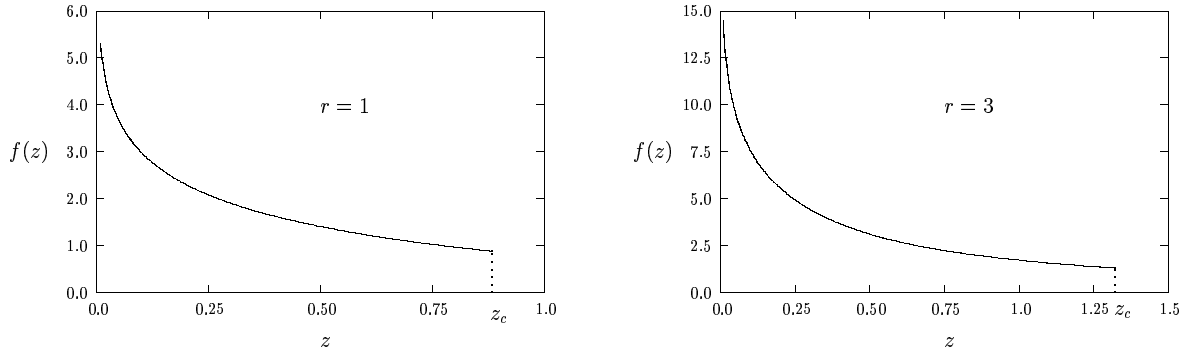


(a) $\tilde{z} = f(z)$ for $r = 1$ (b) $\tilde{z} = f(z)$ for $r = 3$

Figure 3: Plots of the function $\tilde{z} = f(z)$ versus $z$ on the interval $(0, z_c]$ for $r = 1$ and $r = 3$.

We refer to solutions of length $l$ and $\tilde{l}$ as A-type and B-type spikes, respectively. Since $\tilde{l} > l$ and $G_l(0;0)$ is a decreasing function of $l$ as seen from (2.8), it follows from (2.9) and (2.2) that $h(0)$ and $a(0)$ are increasing functions of $l$. Hence, the maximum value of $a$ associated with an A-type spike is smaller than that for a B-type spike. Thus, we refer to A-type and B-type spikes as small and large spikes, respectively.

We now construct $k$-spike equilibrium solutions to (1.1) on the interval $[-1, 1]$ with $k_1 > 0$ spikes of type A and $k_2 = k - k_1 > 0$ spikes of type B arranged in any particular order from left to

right across the interval as

$$\text{ABAAB....B}\,, \qquad k_1 \ - \ \text{A's}\,, \qquad k_2 \ - \ \text{B's}. \tag{2.18}$$

To do so, we use translation invariance and the fact that $h(l) = h(\tilde{l})$ to glue A and B type spikes together to satisfy $C^1$ continuity for the global function $h$ defined on $[-1, 1]$. The global function $a$ is exponentially close to being $C^1$ continuous since the local function is such that $a(l)$ and $a(\tilde{l})$ are exponentially small when $\varepsilon \ll 1$.

Since the support of an A-spike and a B-spike is $2l$ and $2\tilde{l}$, respectively, we get the length constraint $2k_1 l + 2k_2\tilde{l} = 2$. This condition can be written as

$$k_1 z + k_2 \tilde{z} = \sqrt{\mu/D}\,. \tag{2.19a}$$

The other condition that ensures that $h$ is $C^1$ continuous is

$$b(z) = b(\tilde{z})\,. \tag{2.19b}$$

Equation (2.19) is a coupled system for $z$ and $\tilde{z}$. The lengths are given in terms of this solution by

$$l = z\sqrt{D/\mu}\,, \qquad \tilde{l} = \tilde{z}\sqrt{D/\mu}\,. \tag{2.20}$$

We now determine conditions for which (2.19) has a solution on the interval $z \in (0, z_c)$ and $\tilde{z} \in (z_c, \infty)$. The solution to (2.19b) is $\tilde{z} = f(z)$. Hence, we need only look at the intersection points of the inverse function $\tilde{z} = f(z)$ and the straight line $\tilde{z} = -k_1 z/k_2 + k_2^{-1}\sqrt{\mu/D}$ on the interval $z \in (0, z_c)$ and $\tilde{z} \in (z_c, \infty)$. The properties of $f(z)$ listed below (2.15) show that there are two different cases to consider

$$\text{Case (i)} \quad k_1/k_2 \le 1\,; \qquad \text{Case (ii)} \quad k_1/k_2 > 1\,. \tag{2.21}$$

Since $f(z)$ is convex and $f'(z) \le -1$ on $z \in (0, z_c]$, with equality only when $z = z_c$, we can readily obtain the following result:

**Result 2.3**: *Let $r > 0$ and $k_1/k_2 \le 1$. Then, when $D < D_m$, there exists a unique solution $(z, \tilde{z})$ to (2.19) on $z \in (0, z_c)$ and $\tilde{z} \in (z_c, \infty)$, where*

$$D_m = \frac{\mu}{k^2 z_c^2}\,, \qquad k = k_1 + k_2\,, \tag{2.22}$$

*and $z_c$ satisfies (2.14). When $D = D_m$, then $z = \tilde{z} = z_c$ and hence $l = \tilde{l} = 1/k$. In this case, we get a symmetric $k$-spike solution with spikes of equal height.*

**Result 2.4**: *Let $r > 0$ and $k_1/k_2 > 1$. Then, there exists a critical value $D_{m_1} > D_m$ such that the solution multiplicity for (2.19) on the interval $z \in (0, z_c)$ and $\tilde{z} \in (z_c, \infty)$ is as follows:*

$$\begin{aligned} &\text{If } D > D_{m_1} \quad \rightarrow \quad \textit{no solutions}\,, \\ &\text{If } D_m < D < D_{m_1} \quad \rightarrow \quad \textit{exactly two solutions}\,, \\ &\text{If } D < D_m \quad \rightarrow \quad \textit{exactly one solution}\,. \end{aligned} \tag{2.23}$$

*The critical value $D_{m_1}$ is the solution of the tangency condition system*

$$-\frac{k_1}{k_2} z + \sqrt{\frac{\mu}{D}}\frac{1}{k_2} = f(z)\,, \qquad -\frac{k_1}{k_2} = f'(z)\,. \tag{2.24}$$

When $r = 1$, the result 2.4 is illustrated graphically in Fig. 4 in the $\tilde{z}$, $z$ plane. A similar plot could be done for any $r > 0$. When $k_1/k_2 > 1$ and $D$ is decreased from a large value, the straight line of slope $-k_1/k_2$ first intersects the curve $\tilde{z} = f(z)$ at a point of tangency at some critical value of $D$, labeled by $D_{m_1}$. As $D$ is decreased slightly below $D_{m_1}$, there are exactly two roots to (2.19) until $D$ is decreased to the value $D_m$ defined in (2.22). When $D$ is decreased below $D_m$ there is only one solution to (2.19).

For an arbitrary value of $r$, the value $D_{m_1}$ must be calculated numerically using Newton's method. However, when $r = 1$, we can use (2.17) in (2.24) to obtain the explicit result

$$D_{m_1} = \mu \left[ k_1 \sinh^{-1}\left(\frac{k_2}{k_1}\right) + k_2 \sinh^{-1}\left(\frac{k_1}{k_2}\right)\right]^{-2}\,, \qquad \text{for} \quad k_1/k_2 > 1\,, \quad r = 1\,. \tag{2.25}$$

After determining the values of $l$ and $\tilde{l}$ from (2.19) and (2.20) we can obtain an asymmetric spike solution to (1.1) of the symbolic form shown in (2.18). With a slight change of notation, the equilibrium result is summarized as follows:

**Proposition 2.1**: *Let $r > 0$ and $\varepsilon \to 0$. Then, for $D < D_m$, there exists an asymmetric $k$-spike equilibrium solution $(a_e, h_e)$ to (1.1) of the form,*

$$a_e(x) \sim \sum_{j=1}^{k} \left[h_{l_j}\right]^{\gamma} u_c\left[\varepsilon^{-1}(x - x_j)\right]\,, \tag{2.26a}$$

*where $\gamma = q/(p-1)$. The value $h_{l_j}$ of $h$ at the center of the $j^{th}$ spike satisfies*

$$h_{l_j} = \left( \frac{2\sqrt{\mu D}\,\tanh\left(l_j\sqrt{\mu/D}\right)}{\int_{-\infty}^{\infty}[u_c(y)]^m\,dy} \right)^{r}\,. \tag{2.26b}$$

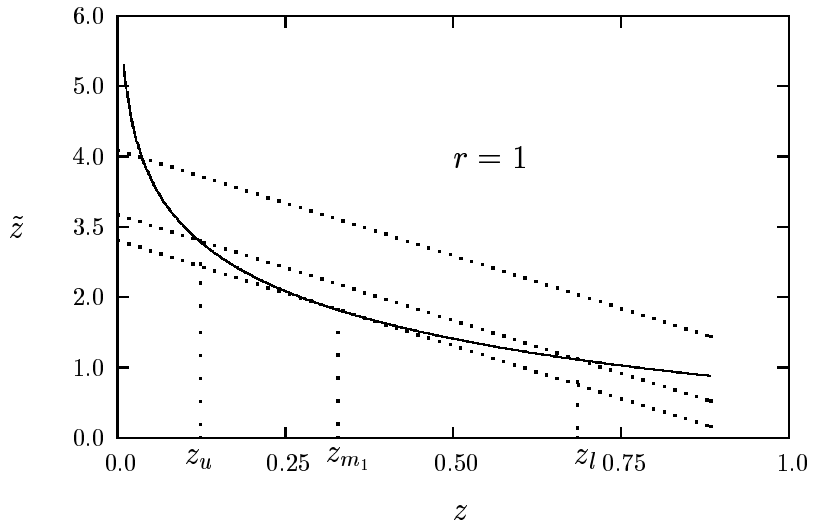


Figure 4: Plot of the graphical solution to (2.19) when $r = 1$, $k_1 = 3$, $k_2 = 1$ and $\mu = 1$. The curve $\tilde{z} = f(z)$ (solid) is plotted together with the straight line (2.19a) (dotted). The line is plotted for three values of $D$: $D = D_{m_1} = .1275$, $D = 0.1$ and $D = 0.06$. When $D = D_{m_1}$ the line is tangent to $f(z)$. When $D = 0.1$ there are two solutions $z_l$ and $z_u$ to (2.19), and only one solution when $D = 0.06$.

*Here for each $j$, $l_j = l$ or $l_j = \tilde{l}$, where $l$ and $\tilde{l}$ are determined in terms of $k_1$, $k_2$ and $\sqrt{\mu/D}$ by (2.19) and (2.20). The value $l_j = l$ must occur $k_1 > 0$ times, while $l_j = \tilde{l}$ must occur $k_2 = k - k_1 > 0$ times. The small and large spikes can be arranged in any sequence. Finally, the equilibrium $h_e$ is*

$$h_e(x) \sim \sum_{j=1}^{k} 2\sqrt{\mu D}\tanh\left(l_j\sqrt{\mu/D}\right) h_{l_j}\; G(x;x_j)\,, \tag{2.27}$$

*where $G(x;x_j)$ satisfies*

$$DG_{xx} - \mu G = -\delta(x - x_j)\,, \qquad -1 < x < 1\,, \tag{2.28a}$$

$$G_x(\pm 1; x_j) = 0\,. \tag{2.28b}$$

*The spike locations $x_j$ are found from*

$$x_1 = l_1 - 1\,, \qquad x_k = 1 - l_k\,, \qquad x_{j+1} = x_j + l_{j+1} + l_j\,, \quad j = 1,..,k-2\,. \tag{2.29}$$

*When $k_1/k_2 > 1$ and $D_m < D < D_{m_1}$, this result still holds. However, as discussed in result 2.4, there are two possible values of the pair $l$ and $\tilde{l}$ for each $D$ on this range.*

To summarize, consider a particular fixed ordering of small and large spikes across the interval. When $D < D_m$, and when there are more large B-spikes than small A-spikes, there is exactly one asymmetric pattern with that particular ordered sequence. However, when there are more small spikes than large spikes in the sequence, then for some range of $D$ there are exactly two such patterns that have the same ordering.

Using Newton's method on (2.24) we can obtain numerical ranges of $D$ for the existence of asymmetric spikes with $k_1 > k_2$. For solutions with three spikes we obtain the following results for $D_m$ and $D_{m_1}$ defined in (2.23):

**Result 2.5 (Three Spikes):** *Let $k_1 = 2$ and $k_2 = 1$. Then,*

$$D_{m_1} = 0.1724 \quad \text{and} \quad D_m = 0.1430\,, \qquad \text{when} \quad r = 1\,, \tag{2.30a}$$

$$D_{m_1} = 0.0732 \quad \text{and} \quad D_m = 0.0641\,, \qquad \text{when} \quad r = 3\,. \tag{2.30b}$$

The corresponding result for four spikes is:

**Result 2.6 (Four Spikes):** *Let $k_1 = 3$ and $k_2 = 1$. Then,*

$$D_{m_1} = 0.1275 \quad \text{and} \quad D_m = 0.0805\,, \qquad \text{when} \quad r = 1\,, \tag{2.31a}$$

$$D_{m_1} = 0.0501 \quad \text{and} \quad D_m = 0.0360\,, \qquad \text{when} \quad r = 3\,. \tag{2.31b}$$

As a remark, there is an interesting scaling result as seen from (2.24). Fix $r$ and the ratio $k_1/k_2$ with $k_1/k_2 > 1$. Let $D^*_{m_1}$ be the largest value of $D$ for which the solution to (2.19) exists when $k_2 = 1$. Then, for any other value of $k_2$, the existence value $D_{m_1}$ is simply $D_{m_1} = D^*_{m_1}/k_2^2$.

In §4 we will show how these asymmetric solutions provide connections between various branches of symmetric $k$-spike solutions. To do so, it is convenient to characterize $h$ in a different way. Let $h(x_j) = h_{l_j}$, where $h_{l_j}$ and $x_j \in (-1, 1)$ are, for the moment, arbitrary. Then, substituting (2.26a) into (1.1b), we get that $h$ satisfies

$$Dh_{xx} - \mu h = -\sum_{j=1}^{k} h_{l_j}^{\gamma m - s} \delta(x - x_j) \quad \left( \int_{-\infty}^{\infty} u_c^m \, dy \right) . \tag{2.32}$$

The equilibrium values for $h_{l_j}$ and $x_j$ are obtained by setting $h(x_j) = h_{l_j}$ and by imposing the symmetry condition $h'(x_{j^+}) + h'(x_{j^-}) = 0$ for $j = 1, .., k$. Solving (2.32) with $h_x(\pm 1) = 0$, and imposing these conditions across $x = x_j$, we obtain a nonlinear system of degree $2k$ for $h_{l_j}$ and $x_j$

$$h_{l_i} = \sum_{j=1}^{k} h_{l_j}^{\gamma m - s} G(x_i; x_j) \left( \int_{-\infty}^{\infty} u_c^m \, dy \right) , \qquad i = 1, .., k , \tag{2.33a}$$

$$h_{l_i}^{\gamma m - s} \left[ G_x(x_{i^+}; x_i) + G_x(x_{i^-}; x_i) \right] + 2 \sum_{\substack{j=1 \\ j \neq i}}^{k} h_{l_j}^{\gamma m - s} G_x(x_i; x_j) = 0 , \qquad i = 1, .., k , \tag{2.33b}$$

where $G$ satisfies (2.28). The asymmetric spike patterns constructed above satisfy this system identically.

The system (2.33) is also satisfied by the symmetric $k$-spike solutions where $h_{l_j} = H$, with $H$ independent of $j$ (see [5]). The spike locations for these solutions are

$$x_j = -1 + \frac{2j - 1}{k} , \qquad j = 1, .., k . \tag{2.34}$$

From [5], it was found for each $i$ that

$$\sum_{j=1}^{k} G(x_i; x_j) = \frac{1}{2\sqrt{\mu D}} \coth \left( \sqrt{\frac{\mu}{D}} \frac{1}{k} \right) . \tag{2.35}$$

Equation (2.33b) is satisfied identically when $h_{l_j} = H$ and when $x_j$ is given by (2.34). Finally, from (2.33a) and (2.35), we can determine $H$ as

$$H^{\gamma m - (1+s)} = 2\sqrt{\mu D} \tanh \left( \sqrt{\frac{\mu}{D}} \frac{1}{k} \right) \left( \int_{-\infty}^{\infty} u_c^m \, dy \right)^{-1} . \tag{2.36}$$

In §4, we will plot the $L_1$ norm of $a$ defined by

$$|a|_1 \equiv \sum_{j=1}^{k} h_{l_j}^{\gamma}\,, \tag{2.37}$$

as a function of $D$ for both symmetric and asymmetric $k$-spike patterns.

# 3 The Stability Analysis: Large Eigenvalues

We now examine the stability of the asymmetric solutions $a_e$ and $h_e$ constructed in §2. We substitute

$$a(x,t) = a_e(x) + e^{\lambda t}\phi(x)\,, \qquad h(x,t) = h_e(x) + e^{\lambda t}\eta(x)\,, \tag{3.1}$$

into (1.1) where $\eta \ll 1$ and $\phi \ll 1$. This leads to the eigenvalue problem

$$\varepsilon^2\phi_{xx} - \phi + \frac{pa_e^{p-1}}{h_e^q}\phi - \frac{qa_e^p}{h_e^{q+1}}\eta = \lambda\phi\,, \qquad -1 < x < 1\,, \tag{3.2a}$$

$$D\eta_{xx} - \mu\eta = -\varepsilon^{-1}m\frac{a_e^{m-1}}{h_e^s}\phi + \varepsilon^{-1}s\frac{a_e^m}{h_e^{s+1}}\eta\,, \qquad -1 < x < 1\,, \tag{3.2b}$$

$$\phi_x(\pm 1) = \eta_x(\pm 1) = 0\,. \tag{3.2c}$$

The spectrum of (3.2) contains large eigenvalues that are $O(1)$ and small eigenvalues that are $O(\varepsilon^2)$ as $\varepsilon \to 0$. The goal is to determine the conditions under which both sets of eigenvalues have negative real parts.

In this section we analyze the large eigenvalues and in §5 we study the small eigenvalues. In §3.1 we consider the case $s = 0$ and in §3.2 we extend the analysis to treat $s > 0$. In the notation below, the subscripts such as $\eta_x$ shall indicate derivatives with respect to $x$ whereas the primes will indicate differentiation with respect to the stretched variable $y$.

## 3.1 The Analysis for $s = 0$

We look for an eigenfunction of (3.2) in the form

$$\phi(x) \sim \sum_{j=1}^{k} \phi_j\left[\varepsilon^{-1}(x - x_j)\right]\,, \tag{3.3}$$

where $\phi_j(y) \to 0$ exponentially as $|y| \to \infty$. Then, the right-hand side of (3.2b) with $s = 0$ behaves like a sum of delta functions when $\varepsilon \ll 1$. Since $h(x_j) = h_{l_j}$, (3.2b) with $s = 0$ becomes

$$D\eta_{xx} - \mu\eta = -\sum_{j=1}^{k} m h_{l_j}^{\gamma(m-1)} \int_{-\infty}^{\infty} u_c^{m-1} \phi_j \, dy \; \delta(x - x_j) \, . \tag{3.4}$$

It is convenient to write $h_{l_j}^{\gamma(m-1)}$ as $h_{l_j}^{\gamma(m-1)} = h_{l_j}^{\gamma m-1} h_{l_j}^{1-\gamma}$. Then, using (2.26b) for $h_{l_j}^{\gamma m-1}$, we get

$$h_{l_j}^{\gamma(m-1)} = \left( \frac{2\sqrt{\mu D} \tanh\left(l_j \sqrt{\mu/D}\right)}{\int_{-\infty}^{\infty} [u_c(y)]^m \, dy} \right) h_{l_j}^{1-\gamma} \, . \tag{3.5}$$

We substitute (3.5) into (3.4) to obtain

$$\eta(x) = \sum_{j=1}^{k} G(x; x_j) \omega_j \, , \tag{3.6}$$

where

$$\omega_j = 2m\sqrt{\mu D} \tanh\left(l_j \sqrt{\mu/D}\right) h_{l_j}^{1-\gamma} \left( \frac{\int_{-\infty}^{\infty} u_c^{m-1} \phi_j \, dy}{\int_{-\infty}^{\infty} u_c^m \, dy} \right) \, . \tag{3.7}$$

Here $G(x; x_j)$ satisfies (2.28).

Next, we substitute (2.26), (2.27), and (3.3) into (3.2a), and let $\varepsilon \to 0$ to obtain the eigenvalue problem

$$\phi_j'' - \phi_j + p u_c^{p-1} \phi_j - q h_{l_j}^{\gamma-1} u_c^p \eta(x_j) = \lambda \phi_j \, , \qquad -\infty < y < \infty \, , \tag{3.8}$$

with $\phi_j(y) \to 0$ as $y \to \infty$. We introduce the notation

$$\mathcal{G} \equiv \begin{pmatrix} G(x_1; x_1) & \cdots & G(x_1; x_k) \\ \vdots & \ddots & \vdots \\ G(x_k; x_1) & \cdots & G(x_k; x_k) \end{pmatrix} \, , \quad \boldsymbol{\omega} \equiv \begin{pmatrix} \omega_1 \\ \vdots \\ \omega_k \end{pmatrix} \, , \quad \boldsymbol{\phi} \equiv \begin{pmatrix} \phi_1 \\ \vdots \\ \phi_k \end{pmatrix} \, , \quad \boldsymbol{\eta} \equiv \begin{pmatrix} \eta(x_1) \\ \vdots \\ \eta(x_k) \end{pmatrix} \, . \tag{3.9}$$

Then, since $\boldsymbol{\eta} = \mathcal{G}\boldsymbol{\omega}$ from (3.6), we can write (3.8) in vector form as

$$\boldsymbol{\phi}'' - \boldsymbol{\phi} + p u_c^{p-1} \boldsymbol{\phi} - q u_c^p \mathcal{H}^{\gamma-1} \mathcal{G} \boldsymbol{\omega} = \lambda \boldsymbol{\phi} \, , \tag{3.10}$$

where $\mathcal{H}$ is the diagonal matrix

$$\mathcal{H} \equiv \begin{pmatrix} h_{l_1} & 0 & \cdots & 0 \\ 0 & \ddots & \cdots & 0 \\ \vdots & \vdots & \ddots & \vdots \\ 0 & 0 & \cdots & h_{l_k} \end{pmatrix} . \tag{3.11}$$

In terms of $\mathcal{H}$, $\boldsymbol{\omega}$ in (3.7) can be written as

$$\boldsymbol{\omega} = m\sqrt{\mu D}\,\mathcal{C}\,\mathcal{H}^{1-\gamma} \left( \frac{\int_{-\infty}^{\infty} u_c^{m-1} \boldsymbol{\phi}\, dy}{\int_{-\infty}^{\infty} u_c^m dy} \right) , \tag{3.12}$$

where the diagonal matrix $\mathcal{C}$ is defined by

$$\mathcal{C} \equiv \begin{pmatrix} 2\tanh z_1 & 0 & \cdots & 0 \\ 0 & \ddots & \cdots & 0 \\ \vdots & \vdots & \ddots & \vdots \\ 0 & 0 & \cdots & 2\tanh z_k \end{pmatrix} , \qquad z_j \equiv l_j \sqrt{\mu/D}\,. \tag{3.13}$$

Substituting (3.12) into (3.10), we obtain the eigenvalue problem

$$\boldsymbol{\phi}'' - \boldsymbol{\phi} + p u_c^{p-1} \boldsymbol{\phi} - mq u_c^p \left( \frac{\int_{-\infty}^{\infty} u_c^{m-1} \mathcal{E} \boldsymbol{\phi}\, dy}{\int_{-\infty}^{\infty} u_c^m\, dy} \right) = \lambda \boldsymbol{\phi}\,, \qquad -\infty < y < \infty\,, \tag{3.14a}$$

$$\boldsymbol{\phi} \to 0\,, \quad \text{as} \quad |y| \to \infty\,. \tag{3.14b}$$

Here the matrix $\mathcal{E}$ is defined by

$$\mathcal{E} = \sqrt{\mu D}\,\mathcal{H}^{\gamma-1} \mathcal{G} \mathcal{C} \mathcal{H}^{1-\gamma}\,. \tag{3.15}$$

Clearly, since $\mathcal{H}$ is invertible, the eigenvalues of $\mathcal{E}$ are the same as those of $\sqrt{\mu D}\mathcal{G}\mathcal{C}$. Since $\mathcal{G}$ is a Green's function matrix it is symmetric positive-definite, and $\mathcal{C}$ is a positive diagonal matrix, Thus, $\mathcal{E}$ has real positive eigenvalues. We write $\mathcal{E}$ as

$$\mathcal{E} = \mathcal{S}^{-1} \Lambda_e \mathcal{S}\,, \tag{3.16}$$

for some nonsingular matrix $\mathcal{S}$. Then, upon defining $\boldsymbol{\psi} = \mathcal{S}\boldsymbol{\phi}$, we obtain from (3.14) that

$$\boldsymbol{\psi}'' - \boldsymbol{\psi} + p u_c^{p-1} \boldsymbol{\psi} - mq u_c^p \left( \frac{\int_{-\infty}^{\infty} u_c^{m-1} \Lambda_e \boldsymbol{\psi}\, dy}{\int_{-\infty}^{\infty} u_c^m\, dy} \right) = \lambda \boldsymbol{\psi}\,, \qquad -\infty < y < \infty\,, \tag{3.17a}$$

$$\boldsymbol{\psi} \to 0\,, \quad \text{as} \quad |y| \to \infty\,. \tag{3.17b}$$

Since $\Lambda_e$ is a diagonal matrix we get $k$ uncoupled scalar problems from (3.17).

The next step is to determine the conditions for which $\mathrm{Re}(\lambda) < 0$ in (3.17). For this we need the following key result of Wei [13]:

**Theorem(Wei [13])**: *Let $\beta > 0$ and consider the nonlocal eigenvalue problem for $\phi(y)$*

$$\phi'' - \phi + p u_c^{p-1}\phi - \beta(p-1)u_c^p \left( \frac{\int_{-\infty}^{\infty} u_c^{m-1}\phi\, dy}{\int_{-\infty}^{\infty} u_c^m dy} \right) = \lambda\phi\,, \qquad -\infty < y < \infty\,, \tag{3.18a}$$

$$\phi \to 0 \quad \text{as} \quad |y| \to \infty\,, \tag{3.18b}$$

*corresponding to eigenpairs for which $\lambda \neq 0$. Here $u_c(y)$ satisfies (2.3). Let $\lambda_0 \neq 0$ be the eigenvalue of (3.18) with the largest real part. Then, if $\beta < 1$, we have*

$$\mathrm{Re}(\lambda_0) > 0\,. \tag{3.19}$$

*Alternatively, if $\beta > 1$ and if either of the following two conditions hold*

$$\text{(i)} \quad m = 2\,,\ 1 < p \le 5\,, \qquad \text{or} \qquad \text{(ii)} \quad m = p+1\,,\ p > 1\,, \tag{3.20a}$$

*then*

$$\mathrm{Re}(\lambda_0) < 0\,. \tag{3.20b}$$

The proof of (3.20) is given in Lemma A and Theorem 1.4 of [13]. The simple proof of (3.19) is given in Appendix E of [5]. The assumption (3.20a) holds for the parameter sets given in (2.13). By comparing (3.17) with (3.18) we obtain the following result on the spectrum of (3.17):

**Proposition 3.1**: *Let $\lambda_0 \neq 0$ be the eigenvalue of (3.17) with the largest real part and assume condition (3.20a) holds. Let $\alpha_1$ be the minimum eigenvalue of the matrix $\mathcal{E}$ defined in (3.15). Then, $Re(\lambda_0) > 0$ when*

$$\alpha_1 < \frac{(p-1)}{qm}\,. \tag{3.21}$$

*Also, $Re(\lambda_0) < 0$ when $\alpha_1 > (p-1)/qm$.*

Thus, we must calculate the minimum eigenvalue of $\mathcal{E}$ as a function of the ordering of the spike pattern, and of $k_1$, $k_2$, $\mu$, $D$ and $r$. In general, since $\mathcal{E}$ is a full matrix, this must be done numerically. However, by finding an alternative representation for the matrix $\mathcal{G}$ in (3.15), we can show that $\mathcal{E}^{-1}$ is a tridiagonal matrix . This will greatly facilitate the numerical implementation of our stability condition.

In Appendix A, we show that

$$\mathcal{G} = \frac{\mathcal{B}^{-1}}{\sqrt{\mu D}}, \tag{3.22}$$

where $\mathcal{B}$ is the tridiagonal matrix

$$\mathcal{B} \equiv \begin{pmatrix} c_1 & d_1 & 0 & \cdots & 0 & 0 & 0 \\ d_1 & c_2 & \ddots & \ddots & \ddots & 0 & 0 \\ 0 & \ddots & \ddots & \ddots & \ddots & \ddots & 0 \\ \vdots & \ddots & \ddots & \ddots & \ddots & \ddots & \vdots \\ 0 & \ddots & \ddots & \ddots & \ddots & \ddots & 0 \\ 0 & 0 & \ddots & \ddots & \ddots & c_{k-1} & d_{k-1} \\ 0 & 0 & 0 & \cdots & 0 & d_{k-1} & c_k \end{pmatrix}, \tag{3.23a}$$

with matrix entries defined by

$$c_1 = \coth(z_1 + z_2) + \tanh z_1\,; \qquad c_k = \coth(z_k + z_{k-1}) + \tanh z_k\,, \tag{3.23b}$$

$$c_j = \coth(z_{j+1} + z_j) + \coth(z_j + z_{j-1})\,, \quad j = 2, .., k-1\,; \quad d_j = -\mathrm{csch}(z_j + z_{j+1})\,, \quad j = 1, .., k-1\,. \tag{3.23c}$$

Here $z_j$ is defined in (3.13).

Substituting (3.22) into the definition of $\mathcal{E}$ in (3.15), we get

$$\mathcal{E} = \mathcal{H}^{\gamma-1}\mathcal{B}^{-1}\mathcal{C}\mathcal{H}^{1-\gamma}\,. \tag{3.24}$$

Since $\mathcal{B}$ is tridiagonal it is more convenient to express Proposition 3.1 in terms of the maximum eigenvalue of $\mathcal{E}^{-1}$. Since $\mathcal{E}^{-1}$ has the same eigenvalues as $\mathcal{C}^{-1}\mathcal{B}$, proposition 3.1 can be written as the following simple criterion:

**Corollary 3.1**: *Let $\lambda_0 \neq 0$ be the eigenvalue of (3.17) with the largest real part and assume condition (3.20a) holds. Let $e_m$ be the maximum eigenvalue of the tridiagonal matrix $\tilde{\mathcal{E}}$ defined by $\tilde{\mathcal{E}} \equiv \mathcal{C}^{-1}\mathcal{B}$. Then, $Re(\lambda_0) > 0$ when*

$$e_m > \frac{qm}{(p-1)}\,. \tag{3.25}$$

*Also, $Re(\lambda_0) < 0$ when $e_m < qm/(p-1)$.*

### 3.2 The Analysis for $s > 0$

The analysis here is more intricate than for the $s = 0$ case. Substituting (3.3), (2.26), and (2.27) into (3.2b), we obtain in place of (3.4) that

$$D\eta_{xx} - \mu\eta = -\sum_{j=1}^{k} \left( m h_{l_j}^{\gamma(m-1)-s} \int_{-\infty}^{\infty} u_c^{m-1} \phi_j \, dy - s h_{l_j}^{\gamma m-(s+1)} \int_{-\infty}^{\infty} u_c^m \, dy \, \eta(x_j) \right) \delta(x - x_j) \,. \tag{3.26}$$

Then, using (2.26b) for $h_{l_j}$ we can write (3.26) as

$$D\eta_{xx} - \left[ \mu + 2s\sqrt{\mu D} \sum_{j=1}^{k} \tanh\left( l_j \sqrt{\frac{\mu}{D}} \right) \delta(x - x_j) \right] \eta = -\sum_{j=1}^{k} \omega_j \delta(x - x_j) \,, \tag{3.27}$$

where $\omega_j$ was defined in (3.7). Thus, we obtain

$$D\eta_{xx} - \mu\eta = 0 \,; \qquad \eta_x(\pm 1) = 0 \,, \tag{3.28a}$$

$$[\eta]_j = 0 \,, \qquad [D\eta_x]_j = -\omega_j + 2s\sqrt{\mu D} \tanh(z_j)\eta(x_j) \,. \tag{3.28b}$$

By solving this system as in Appendix A, we can readily show that $\boldsymbol{\eta}$ satisfies the linear system

$$(\mathcal{B} + s\mathcal{C})\, \boldsymbol{\eta} = \frac{\boldsymbol{\omega}}{\sqrt{\mu D}} \,, \tag{3.29}$$

where $\mathcal{B}$ and $\mathcal{C}$ were defined in (3.23) and (3.13), respectively. Substituting (3.7) for $\boldsymbol{\omega}$ into (3.29), we get

$$\boldsymbol{\eta} = m \left( \mathcal{B} + s\mathcal{C} \right)^{-1} \mathcal{C} \mathcal{H}^{1-\gamma} \left( \frac{\int_{-\infty}^{\infty} u_c^{m-1} \boldsymbol{\phi} \, dy}{\int_{-\infty}^{\infty} u_c^m \, dy} \right) . \tag{3.30}$$

Equation (3.8) for the eigenvalue problem for $\phi_j$ still holds. Substituting (3.30) into (3.8) we get (3.14) where, in place of (3.15), $\mathcal{E}$ is now defined by

$$\mathcal{E} = \mathcal{H}^{\gamma-1} \left( \mathcal{B} + s\mathcal{C} \right)^{-1} \mathcal{C} \mathcal{H}^{1-\gamma} \,. \tag{3.31}$$

The stability criterion in Proposition 3.1 still holds if we identify $\alpha_1$ in (3.21) as the minimum eigenvalue of the matrix $\left( \mathcal{B} + s\mathcal{C} \right)^{-1} \mathcal{C}$. Alternatively, by computing $\mathcal{E}^{-1}$ we can obtain the following result analogous to Corollary 3.1:

**Corollary 3.2**: *Let $\lambda_0 \neq 0$ be the eigenvalue of (3.17) with the largest real part and assume condition (3.20a) holds. Let $e_m$ be the maximum eigenvalue of the tridiagonal matrix $\tilde{\mathcal{E}}$ defined by $\tilde{\mathcal{E}} \equiv \mathcal{C}^{-1}\mathcal{B}$. Then, $Re(\lambda_0) > 0$ when*

$$e_m > 1 + \frac{1}{r}\,. \tag{3.32}$$

*Also, $Re(\lambda_0) < 0$ when $e_m < 1 + r^{-1}$. Here $r$ is defined in (2.12) in terms of $s$.*

Since $r$ is an increasing function of $s$ we conclude that the effect of $s$ is to make it more difficult to stablize an asymmetric spike pattern with respect to the large $O(1)$ eigenvalues.

# 4 Examples of the Theory

We now give some analytical and numerical predictions obtained from our existence and stability criteria for asymmetric patterns with four or fewer spikes. The existence criterion for the asymmetric equilibrium solution did not depend on the specific orientation of the spikes on the interval. However, for solutions with three or more spikes, the critical values of $D$ for stability with respect to the large $O(1)$ eigenvalues do depend on the specific ordering of the spikes.

## 4.1 Two-Spike Patterns

For the case of two spikes where $k_1 = k_2 = 1$ we can find a simple criterion for the critical value $D_e$ at which stability changes. In this case, we can calculate the matrix $\tilde{\mathcal{E}} = \mathcal{C}^{-1}\mathcal{B}$ in Corollary 3.2 analytically. Using (3.23) for $\mathcal{B}$ and (3.13) for $\mathcal{C}$, we get

$$\tilde{\mathcal{E}} = \frac{1}{2}\mathrm{I} + \frac{1}{2}\begin{pmatrix} \coth z_1 \coth(z_1+z_2) & -\coth z_1 \operatorname{csch}(z_1+z_2) \\ -\coth z_2 \operatorname{csch}(z_1+z_2) & \coth z_2 \coth(z_1+z_2) \end{pmatrix}, \tag{4.1}$$

where I is the $2\times 2$ identity matrix. Let $e$ be an eigenvalue of $\tilde{\mathcal{E}}$ and $\sigma$ be an eigenvalue of $\tilde{\mathcal{E}} - (1/2)\mathrm{I}$. Then, using standard identities for hyperbolic functions, we obtain that $\sigma$ satisfies the characteristic equation

$$(2\sigma - 1)\,(2\sigma - \coth z_1 \coth z_2) = 0\,. \tag{4.2}$$

Hence $\tilde{\mathcal{E}}$ has an eigenvalue $e = 1$. The maximum eigenvalue $e_m$ needed in Corollary 3.2 is

$$e_m = \frac{1}{2} + \frac{1}{2}\coth z_1 \coth z_2\,. \tag{4.3}$$

Without loss of generality we can set $z_1 = z$ and $z_2 = \tilde{z}$. Thus, AB patterns have the same stability criterion as do BA patterns. Substituting (4.3) into Corollary 3.2, we get the following result:
**Corollary 4.1(Two Spikes)**: *Let $r > 0$ and $k_1 = k_2 = 1$. Assume that $D$ is such that a two-spike pattern exists, where $z$ and $\tilde{z}$ are computed from (2.19). Then, the pattern is stable with respect to the large $O(1)$ eigenvalues when*

$$\coth z \, \coth \tilde{z} < 1 + 2/r \, , \tag{4.4}$$

*and it is unstable when* $\coth z \, \coth \tilde{z} > 1 + 2/r$. *Here $r$ is defined in (2.12).*

Since $z \to 0$ and $\tilde{z} \to \infty$ as $D \to 0$, condition (4.4) will hold only when $D$ is sufficiently close to $D_m$. Qualitatively, this shows that the pattern becomes unstable when the ratio of the lengths of the regions for the B and the A-type spikes exceeds some critical value. Let $D_e$ be the value of $D$ for which

$$\coth z \, \coth \tilde{z} = 1 + 2/r \, . \tag{4.5}$$

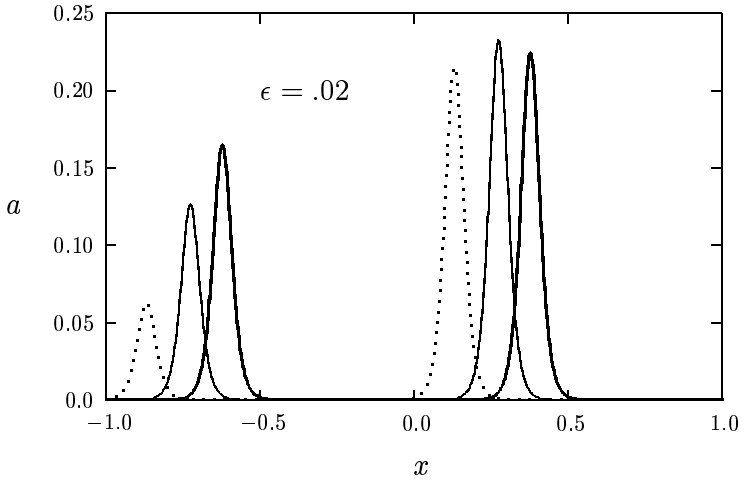


Figure 5: Plot of the activator concentration for a two-spike asymptotic asymmetric equilibrium solution of the form AB with $D = .31$ (heavy solid curve), $D = 0.28$ (solid curve), and $D = .24$ (dotted curve). Also, $\epsilon = .02$, $\mu = 1$ and $(p, q, m, s) = (2, 1, 2, 0)$.

When $r = 1$ we can find $D_e$ analytically. From (2.16) and (2.19a) we get one equation relating

$z$ and $D$. Substituting (2.19a) into (4.5) gives another equation. Hence, $D_e$ is the solution of

$$\sinh z \, \sinh\left(\sqrt{\mu/D} - z\right) = 1\,, \qquad \cosh z \, \cosh\left(\sqrt{\mu/D} - z\right) = 3\,. \tag{4.6a}$$

This system is equivalent to

$$\cosh\left(\sqrt{\mu/D}\right) - \cosh\left(2z - \sqrt{\mu/D}\right) = 2\,, \qquad \cosh\left(\sqrt{\mu/D}\right) + \cosh\left(2z - \sqrt{\mu/D}\right) = 6\,. \tag{4.6b}$$

Thus $D_e$ satisfies $\cosh\left(\sqrt{\mu/D}\right) = 4$. When $r = 3$, we use Newton's method on the coupled system (2.19), (4.5) to find $D_e$ numerically. The existence results of §2 and these stability results are summarized as follows:

**Result 4.1(Two Spikes)**: *Let $k_1 = k_2 = 1$. Then, a two-spike pattern of the form AB or BA exists and is stable with respect to the large $O(1)$ eigenvalues when $D$ satisfies*

$$.2349 \approx \left[\log\left(4 + \sqrt{15}\right)\right]^{-2} < \frac{D}{\mu} < \left[2\log\left(1 + \sqrt{2}\right)\right]^{-2} \approx .3218\,, \qquad \text{for} \quad r = 1\,, \tag{4.7a}$$

$$0.1075 < \frac{D}{\mu} < \left[2\log\left(2 + \sqrt{3}\right)\right]^{-2} \approx .1441\,, \qquad \text{for} \quad r = 3\,. \tag{4.7b}$$

The upper bounds in (4.7) are the existence bounds given in (2.22). The pattern loses its stability when $D$ is decreased below the lower bounds in (4.7).

When $(p, q, m, s) = (2, 1, 2, 0)$, so that $r = 1$, in Fig. 5 we plot the asymptotic activator concentration obtained from proposition 2.1 for AB patterns at three different values of $D$. The values of $D$ shown in this figure all satisfy the stability criterion in (4.7a).

### 4.2 Three-Spike Patterns

Similar results can be obtained for a three-spike pattern. Using (3.23) for $\mathcal{B}$ and (3.13) for $\mathcal{C}$, we get

$$\tilde{\mathcal{E}} = \frac{1}{2}\mathrm{I} + \frac{1}{2}\hat{\mathcal{E}}\,, \qquad \hat{\mathcal{E}} \equiv \begin{pmatrix} e_{11} & e_{12} & 0 \\ e_{21} & e_{22} & e_{23} \\ 0 & e_{32} & e_{33} \end{pmatrix}\,, \tag{4.8a}$$

where the entries $e_{ij}$ are defined by

$$\begin{aligned} &e_{11} = \coth z_1 \, \coth(z_1 + z_2)\,, \quad e_{12} = -\coth z_1 \, \mathrm{csch}(z_1 + z_2)\,, \quad e_{21} = -\coth z_2 \, \mathrm{csch}(z_1 + z_2)\,, \\ &e_{22} = \coth z_2 \, [\coth(z_1 + z_2) + \coth(z_2 + z_3)] - 1\,, \qquad e_{23} = -\coth z_2 \, \mathrm{csch}(z_2 + z_3)\,, \\ &e_{32} = -\coth z_3 \, \mathrm{csch}(z_2 + z_3)\,, \qquad e_{33} = \coth z_3 \, \coth(z_2 + z_3)\,. \end{aligned} \tag{4.8b}$$

Let $e$ and $\sigma$ be an eigenvalue of $\tilde{\mathcal{E}}$ and $\hat{\mathcal{E}}$, respectively. Then, it is straightforward to show that $\sigma = 1$ is an eigenvalue of $\hat{\mathcal{E}}$. With this information, we readily calculate that the other two eigenvalues of $\hat{\mathcal{E}}$ satisfy

$$\sigma^2 - \sigma\,(\kappa_t - 1) + \kappa_d = 0\,. \tag{4.9a}$$

Here $\kappa_t$ and $\kappa_d$ are the trace and determinant of $\hat{\mathcal{E}}$, respectively, given in terms of the $e_{ij}$ by

$$\kappa_t = e_{11} + e_{22} + e_{33}\,, \qquad \kappa_d = e_{11}e_{22}e_{33} - e_{11}e_{23}e_{32} - e_{33}e_{21}e_{12}\,. \tag{4.9b}$$

Thus, the maximum eigenvalue $e_m$ of $\tilde{\mathcal{E}}$ needed in Corollary 3.2 is

$$e_m = \frac{1}{2} + \frac{1}{2}\left([\kappa_t - 1] + \sqrt{[\kappa_t - 1]^2 - 4\kappa_d}\right)\,. \tag{4.10}$$

Substituting (4.10) into (3.32) we obtain the following result analogous to Corollary 4.1:
**Corollary 4.2(Three Spikes)**: *Let $r > 0$ and $k = 3$. Assume that $D$ is such that a three-spike pattern exists, where $z$ and $\tilde{z}$ are computed from (2.19). Then, the pattern is stable with respect to the large $O(1)$ eigenvalues when*

$$\frac{1}{2}\left([\kappa_t - 1] + \sqrt{[\kappa_t - 1]^2 - 4\kappa_d}\right) < 1 + 2/r\,, \tag{4.11}$$

*and it is unstable when the inequality in (4.11) is reversed.*

Let $D_e$ be the value of $D$ for which

$$\frac{1}{2}\left([\kappa_t - 1] + \sqrt{[\kappa_t - 1]^2 - 4\kappa_d}\right) = 1 + 2/r\,, \tag{4.12}$$

Equations (4.12) and (2.19) form a coupled system for $z$, $\tilde{z}$ and $D_e$, which must be solved by Newton's method. This system depends on $k_1$, $k_2$, $r$, and on the specific ordering of the small and large spikes on the interval. However, by examining (4.11), with the $e_{ij}$ as defined in (4.8b), it follows that patterns of the form AAB and BAA have the same stability criterion as well as patterns of the form BBA and ABB.

We first consider the case $k_1 = 1$ and $k_2 = 2$ so that no solution multiplicity occurs. There are two different values of $D_e$ depending on the two orientations ABB and BAB. We obtain the following results:

**Result 4.2(Three Spikes)**: *Let $k_1 = 1$ and $k_2 = 2$. Then, a three-spike pattern exists and is stable with respect to the large $O(1)$ eigenvalues when $D$ satisfies*

$$ABB \quad \rightarrow \quad 0.0711 < \frac{D}{\mu} < 0.1430\,, \quad (r=1)\,; \qquad 0.0345 < \frac{D}{\mu} < 0.0641\,, \quad (r=3)\,, \tag{4.13a}$$

$$BAB \quad \rightarrow \quad 0.1127 < \frac{D}{\mu} < 0.1430\,, \quad (r=1)\,; \qquad 0.0534 < \frac{D}{\mu} < 0.0641\,, \quad (r=3)\,. \tag{4.13b}$$

The three-spike pattern loses its stability when $D$ is decreased below the lower bounds in (4.13). The upper bounds are the values of $D_m$ given in result 2.5.

In Fig. 6(a) and Fig. 6(b) we take $(p, q, m, s) = (2, 1, 2, 0)$ and plot the asymptotic activator concentration from proposition 2.1 for BAB and ABB patterns, respectively. For each pattern we plot the solution at two different values of $D$. From (4.13a) and (4.13b) we see that all of these solutions are stable except for the BAB pattern in Fig. 6(a) with $D = .075$.

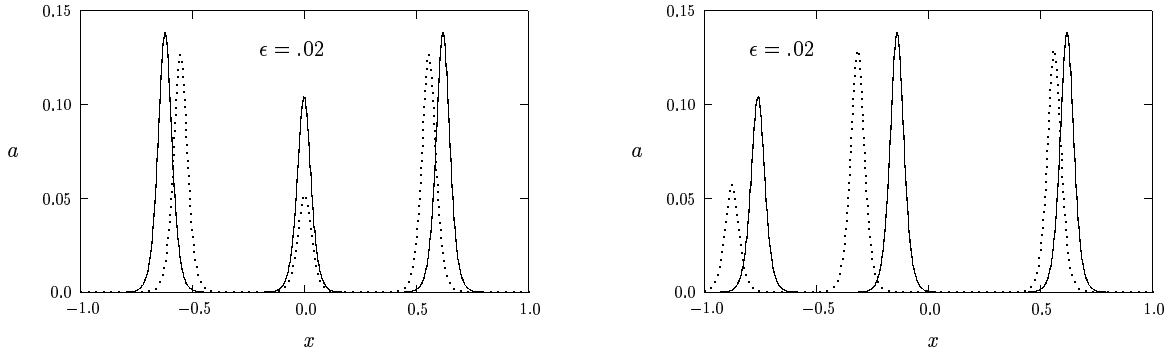


(a) BAB pattern: $D = .12$ (solid curve), $D = 0.075$ (dotted curve)

(b) ABB pattern: $D = .12$ (solid curve), $D = 0.08$ (dotted curve)

Figure 6: Plot of the activator concentration for a three-spike asymptotic asymmetric equilibrium solution of the form BAB and ABB for two different values of $D$ with $\epsilon = .02$, $\mu = 1$ and $(p, q, m, s) = (2, 1, 2, 0)$.

Now we consider the case where $k_1 = 2$ and $k_2 = 1$. In this case, solution multiplicity occurs for the range of $D$ given in result 2.5. There are two patterns to consider: AAB and ABA. To find the critical value $D_e$ of $D$, where the stability of each of these patterns is exchanged, we must solve the coupled system (2.19) and (4.12) numerically. When $r = 1$, the results are illustrated graphically

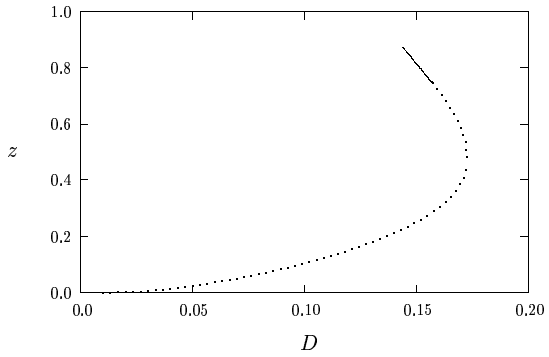


(a) AAB pattern: $D_e = 0.157$

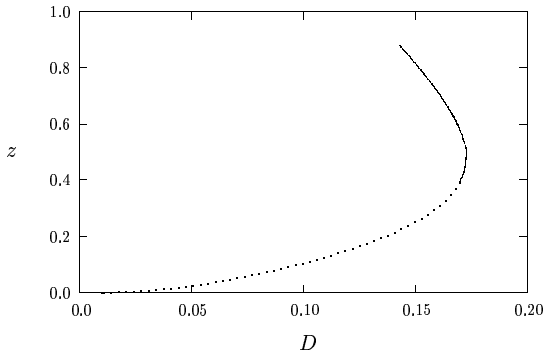


(b) ABA pattern: $D_e = 0.170$

Figure 7: Plots of $z$ versus $D$ exhibiting solution multiplicity for a three-spike pattern with $k_1 = 2$, $k_1$=1, $\mu = 1$ and $(p, q, m, s) = (2, 1, 2, 0)$. The solid (dotted) curve is stable (unstable) with respect to the large $O(1)$ eigenvalues. The critical value $D_e$ where the stability is exchanged is indicated.

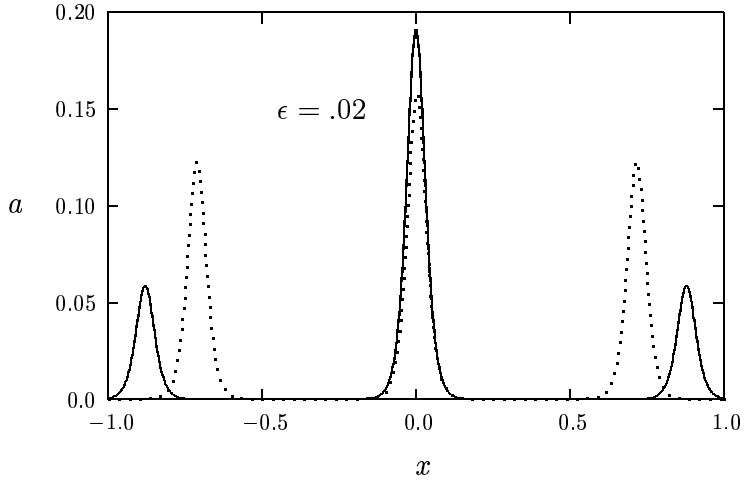


Figure 8: Plot of the activator concentration for a three-spike asymptotic asymmetric equilibrium solution of the form ABA in the region where solution multiplicity occurs. The parameters are $D = 0.16$, $\epsilon = .02$, $\mu = 1$ and $(p, q, m, s) = (2, 1, 2, 0)$. The solid curve corresponds to the smaller root $z_u$ while the dotted curve corresponds to the larger root $z_l$.

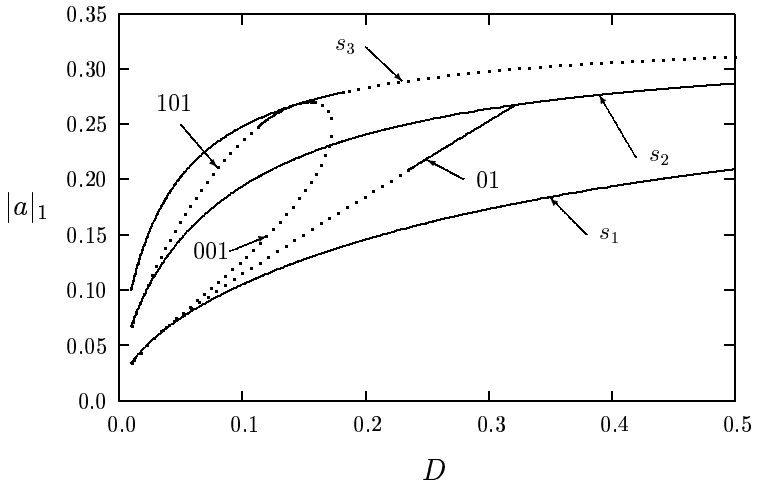


Figure 9: Plot of $|a|_1$ defined in (2.37) versus $D$ for solutions with three or fewer spikes. Here $\mu = 1$ and $(p, q, m, s) = (2, 1, 2, 0)$. The symmetric branch with $k$ spikes is labeled by $s_k$. The asymmetric patterns AB, BAB, and AAB are labeled by 01, 101, and 001, respectively. The portions of the branches that are solid (dotted) are stable (unstable) with respect to the large $O(1)$ eigenvalues.

in Fig. 7(a) and Fig. 7(b), where we plot the solution $z$ to (2.19) as a function of $D$ for the patterns AAB and ABA, respectively. The portion of the branch that is stable is indicated by the solid line. In the caption of each of these figures we give a numerical value for $D_e$. Notice that, in contrast to AAB patterns, the exchange of stability for the more stable ABA patterns occurs on the other side of the fold point in the $z$ versus $D$ diagram. An identical topological situation is found to hold for the case $r = 3$ and we calculate numerically that

$$D_e = .0689 \qquad \text{AAB pattern} \quad r = 3\,; \qquad D_e = .0712 \qquad \text{ABA pattern} \quad r = 3\,. \tag{4.14}$$

In Fig. 8 we plot the two solutions of the form ABA that exist when $D = 0.16$ is chosen to lie in the multiplicity zone with $k_1 = 2$, $k_2 = 1$, and $r = 1$. The dotted curve in this figure, which corresponds to the larger value of $z$ in Fig. 7(b) when $D = 0.16$ is stable. The solid curve in Fig. 8, which corresponds to the smaller value of $z$ when $D = 0.16$, is unstable.

Finally, in Fig. 9 we take $(p, q, m, s) = (2, 1, 2, 0)$ and we plot the bifurcation diagram of the norm $|a|_1$, defined in (2.37), versus $D$ for both the asymmetric solution branches and the symmetric solution branches given in (2.34)–(2.36). From [5], in the limit $\varepsilon \to 0$ and for $r$ defined in (2.12), it was found that the $k$-spike symmetric solution branch was stable with respect to the large $O(1)$

eigenvalues when $D < D_k$, where

$$D_k = 4\mu k^{-2}\left[\ln\left(\beta + \sqrt{\beta^2 - 1}\right)\right]^{-2}, \qquad \beta \equiv 1 + (1 + \cos(\pi/k))\, r\,. \tag{4.15}$$

The portions of these branches that are stable with respect to the large $O(1)$ eigenvalues are given by the solid lines. Notice that the asymmetric patterns provide the connections between the branches of symmetric solutions. In plotting the connecting branches, we note that a pattern such as ABA traces out exactly the same curve in this figure as an AAB pattern, except that their stability properties are different. In each case when drawing a connecting asymmetric branch, we have plotted the one that is maximally unstable (i. e. the one that goes unstable for the largest value of $D$).

### 4.3 Four-Spike Patterns

For the case of four spikes we must find the maximum eigenvalue of $\tilde{\mathcal{E}}$ in Corollary 3.2 numerically using LAPACK [1]. Patterns that have the same stability values of $D_e$ are now AABB and BBAA, BABA and ABAB, AAAB and BAAA, ABBB and BBBA. The numerical results that we obtain for $k_1 \le k_2$ are given in the next result:

**Result 4.3(Four Spikes)**: *Let $k_1 \le k_2$. Then, a four-spike pattern exists and is stable with respect to the large $O(1)$ eigenvalues when $D$ satisfies*

$$ABBB \quad \to \quad 0.0338 < \frac{D}{\mu} < 0.0805\,, \quad (r=1)\,; \qquad 0.0168 < \frac{D}{\mu} < 0.0361\,, \quad (r=3)\,, \tag{4.16a}$$

$$BABB \quad \to \quad 0.0588 < \frac{D}{\mu} < 0.0805\,, \quad (r=1)\,; \qquad 0.0284 < \frac{D}{\mu} < 0.0361\,, \quad (r=3)\,, \tag{4.16b}$$

$$AABB \quad \to \quad 0.0794 < \frac{D}{\mu} < 0.0805\,, \quad (r=1)\,; \qquad 0.0356 < \frac{D}{\mu} < 0.0361\,, \quad (r=3)\,, \tag{4.16c}$$

$$BABA \quad \to \quad 0.0768 < \frac{D}{\mu} < 0.0805\,, \quad (r=1)\,; \qquad 0.0347 < \frac{D}{\mu} < 0.0361\,, \quad (r=3)\,. \tag{4.16d}$$

From this data we conclude that solutions with fewer small spikes have wider stability regions than those with more small spikes.

In Fig. 10(a) and Fig. 10(b) we take $(p, q, m, s) = (2, 1, 2, 0)$ and plot the asymptotic activator concentration for BABA and BABB patterns, respectively. For each pattern we plot the solution at two different values of $D$. From result 4.3 we see that only the solutions corresponding to the larger value of $D$ in each figure are stable.

Next, we let $k_1 = 3$ and $k_2 = 1$, for which solution multiplicity occurs. The only two patterns with different stability criteria are AAAB and AABA. Similar to the three-spike case, we set $r = 1$

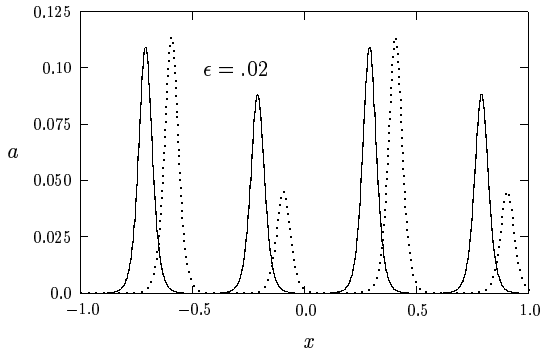


(a) BABA pattern: $D = .079$ (solid curve), $D = 0.06$ (dotted curve)

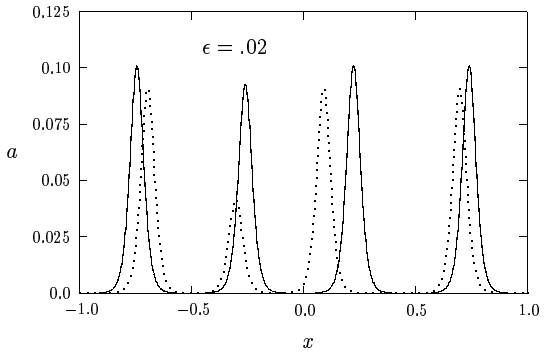


(b) BABB pattern: $D = .075$ (solid curve), $D = 0.04$ (dotted curve)

Figure 10: Plot of the activator concentration for a four-spike asymptotic asymmetric equilibrium solution of the form BABA and BABB for two different values of $D$ with $\epsilon = .02$, $\mu = 1$ and $(p, q, m, s) = (2, 1, 2, 0)$.

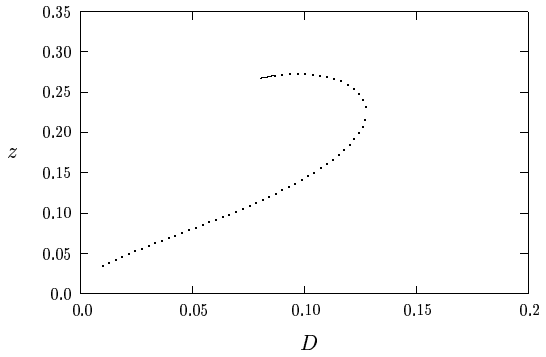


(a) AAAB pattern: $D_e = 0.0865$

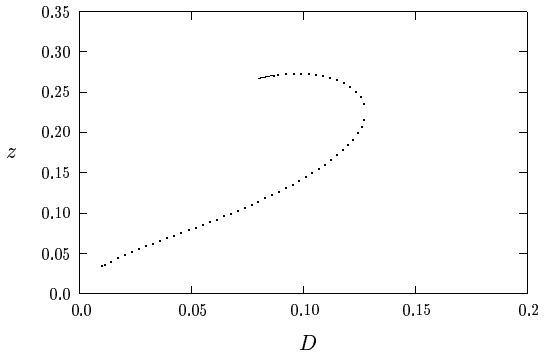


(b) AABA pattern: $D_e = 0.0921$

Figure 11: Plots of $z$ versus $D$ exhibiting solution multiplicity for a four-spike pattern with $k_1 = 3$, $k_1$=1, $\mu = 1$ and $(p, q, m, s) = (2, 1, 2, 0)$. The solid (dotted) curve is stable (unstable) with respect to the large $O(1)$ eigenvalues. The critical value $D_e$ where the stability is exchanged is indicated.

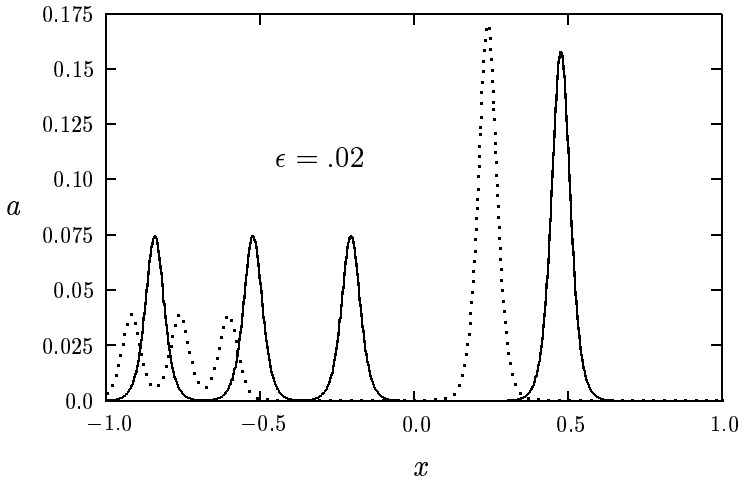


Figure 12: Plot of the activator concentration for a four-spike asymptotic asymmetric equilibrium solution of the form AAAB in the region where solution multiplicity occurs. The parameters are $D = 0.122$, $\epsilon = .02$, $\mu = 1$ and $(p, q, m, s) = (2, 1, 2, 0)$. The solid curve corresponds to the larger root $z_l$ while the dotted curve corresponds to the smaller root $z_u$.

and solve for $z$ as a function of $D$ in (2.19) and numerically identify the values of $D$ for which the stability criterion in Corollary 3.2 is satisfied. The results are shown in Fig. 11(a) and Fig. 11(b) for the AAAB and AABA patterns, respectively. The critical value $D_e$ is shown in the captions. The exchange of stability location is topologically similar when $r = 3$ and for that case the new values of $D_e$ are

$$D_e = .0382 \qquad \text{AAAB pattern} \quad r = 3\,; \qquad D_e = .0402 \qquad \text{AABA pattern} \quad r = 3\,. \tag{4.17}$$

In Fig. 12 we plot the two solutions of the form AAAB that exist when $D = .122$, $k_1 = 3$, $k_2 = 1$, $\mu = 1$ and $(p, q, r, s) = (2, 1, 2, 0)$. Both of these solutions are unstable.

Finally, in Fig. 13 we take $(p, q, m, s) = (2, 1, 2, 0)$ and we plot the bifurcation diagram of the norm $|a|_1$ versus $D$ showing the transitions between the $s_4$ branch and the other symmetric branches with fewer spikes. Similar to that shown in Fig. 9, an asymmetric solution with $m$ small spikes provides the transition between $s_k$ and $s_{k-m}$. As in Fig. 9, the asymmetric branches that we have plotted in Fig. 13 are the maximally unstable branches in the sense defined previously for the three-spike case.

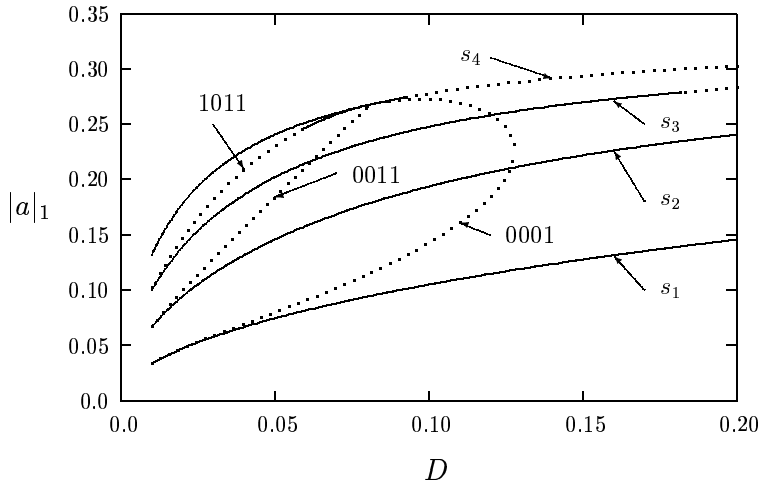


Figure 13: Plot of $|a|_1$ versus $D$ showing the transitions between $s_4$ and the other symmetric branches $s_k$ with $k \leq 3$. Here $\mu = 1$ and $(p, q, m, s) = (2, 1, 2, 0)$. The asymmetric patterns BABB, AABB, and AAAB, are labeled by 1011, 0011, and 0001, respectively. The portions of the branches that are solid (dotted) are stable (unstable) with respect to the large $O(1)$ eigenvalues.

### 4.4 A Few General Results

For $k \leq 4$, it was shown numerically that an asymmetric branch with $m$ small spikes connects the symmetric branches $s_k$ and $s_{k-m}$. Based on further numerical evidence, we believe that this property holds for arbitrary $k$. The stability property of the asymmetric branch that emerges from $s_k$ is given in the next result.

**Result 4.4**: *An asymmetric branch that emerges from the symmetric branch $s_k$ is always stable with respect to the large $O(1)$ eigenvalues for $D - D_m$ sufficiently small.*

To show this result, it suffices to show that $D_k > D_m$, where $D_k$ is the maximum value of $D$ for which the symmetric branch $s_k$ is stable and $D_m$ is the value of $D$ given in (2.22) at which the asymmetric branch emerges from $s_k$. By continuity of matrix eigenvalues with respect to small perturbations of a nonsingular matrix, the result 4.4 follows. Using (2.22) and (4.15), we calculate

$$\frac{1}{D_k} - \frac{1}{D_m} = \frac{k^2}{4\mu}\left[\left(\ln\left[\beta + \sqrt{\beta^2 - 1}\right]\right)^2 - 4\left(\ln\left[\sqrt{r} + \sqrt{r+1}\right]\right)^2\right], \tag{4.18}$$

where $\beta$ was defined in (4.15). For $k \geq 1$ we have that $\beta \in (1, 1 + 2r)$. For this range of $\beta$ it is easy

to see that

$$\beta + \sqrt{\beta^2 - 1} < 2r + 1 + 2\sqrt{r(r+1)}\,. \tag{4.19}$$

Thus, from (4.18) and (4.19), we get the desired result $D_k > D_m$.

The next result concerns an eigenvalue of the stability matrix $\tilde{\mathcal{E}}$ defined in Corollary 3.2.

**Result 4.5**: *The matrix $\tilde{\mathcal{E}} = \mathcal{C}^{-1}\mathcal{B}$ always has the value one as an eigenvalue.*

To show this, we substitute (2.26b) into the equilibrium equation (2.33a). This readily yields

$$\sqrt{\mu D}\,\mathcal{G}\,\mathcal{C}\,\boldsymbol{\xi} = \boldsymbol{\xi}\,, \qquad \boldsymbol{\xi} \equiv \begin{pmatrix} \tanh^r z_1 \\ \vdots \\ \tanh^r z_k \end{pmatrix}. \tag{4.20}$$

The result follows from (4.20) and (3.22), which relates $\mathcal{G}$ and $\mathcal{B}^{-1}$. The eigenvector for $\tilde{\mathcal{E}}$ associated with this eigenvalue is simply $\boldsymbol{\xi}$.

# 5 The Stability Analysis: Small Eigenvalues

The results in §3 establish conditions for which asymmetric spike patterns are stable on an $O(1)$ time scale. However, since there are small eigenvalues of order $O(\varepsilon^2)$, there could be instabilities on a time scale $t = O(\varepsilon^{-2})$. Thus, we must analyze the small eigenvalues and determine the range of $D$ for which they are in the left half-plane. The first step, done in §5.1, is to reduce (3.2) to the study of a matrix eigenvalue problem. This part of the analysis is similar to the one given for symmetric spikes in [5]. In §5.2 we analyze this matrix eigenvalue problem and compute the eigenvalues numerically.

## 5.1 Deriving the Matrix Eigenvalue Problem

We begin by writing (3.2) in the form

$$L_\varepsilon\phi - \frac{qa_e^p}{h_e^{q+1}}\eta = \lambda\phi\,, \qquad -1 < x < 1\,, \tag{5.1a}$$

$$D\eta_{xx} - \mu\eta = -\varepsilon^{-1}m\frac{a_e^{m-1}}{h_e^s}\phi + \varepsilon^{-1}s\frac{a_e^m}{h_e^{s+1}}\eta\,, \qquad -1 < x < 1\,, \tag{5.1b}$$

$$\phi_x(\pm 1) = \eta_x(\pm 1) = 0\,, \tag{5.1c}$$

where

$$L_\varepsilon\phi \equiv \varepsilon^2\phi_{xx} - \phi + \frac{pa_e^{p-1}}{h_e^q}\phi\,. \tag{5.1d}$$

Here $a_e$ and $h_e$ are given by

$$a_e \sim \sum_{j=1}^{k} h_{l_j}^{\gamma} u_j \,; \qquad h_e \sim \sum_{j=1}^{k} 2\sqrt{\mu D}\tanh(z_j) h_{l_j} G(x;x_j) \qquad z_j = l_j\sqrt{\mu/D}\,, \tag{5.2}$$

We have defined $u_j(y) \equiv u_c\left[\varepsilon^{-1}(x-x_j)\right]$, where $u_c(y)$ satisfies (2.3). Also, $h_{l_j}$ and $x_j$ are given in (2.26b) and (2.29), respectively. The $x_j$ are such that

$$\langle h_{ex}\rangle_j = 0\,, \qquad j = 1,..,k\,. \tag{5.3}$$

Here and below we have defined $\langle\zeta\rangle_j \equiv (\zeta(x_{j+}) + \zeta(x_{j-}))/2$ and $[\zeta]_j \equiv \zeta(x_{j+}) - \zeta(x_{j-})$, where $\zeta(x_{j\pm})$ are the one-sided limits of $\zeta(x)$ as $x \to x_{j\pm}$.

If $D$ was infinite and there only one spike, then by translation invariance we would obtain $L_\varepsilon a_{ex} = 0$. Here we expect that $L_\varepsilon a_{ex}$ is still small. To show this, we differentiate the equilibrium problem for (1.1a) with respect to $x$ to get

$$L_\varepsilon a_{ex} = \frac{q a_e^p}{h_e^{q+1}} h_{ex}\,. \tag{5.4}$$

Thus, for $x$ near $x_j$ we get

$$L_\varepsilon u_j^{'} \sim \frac{\varepsilon q h_{l_j}^q u_j^p}{h_e^{q+1}} h_{ex}\,. \tag{5.5}$$

This fact suggests that we expand

$$\phi = \phi_0 + \varepsilon\phi_1 + \cdots\,, \qquad \eta(x) = \varepsilon\eta_0(x) + \cdots\,, \tag{5.6a}$$

where

$$\phi_0 \equiv \sum_{j=1}^{k} c_j u_j^{'}\left[\varepsilon^{-1}(x-x_j)\right]\,, \qquad \phi_1 \equiv \sum_{j=1}^{k} c_j \phi_{1j}\left[\varepsilon^{-1}(x-x_j)\right]\,, \tag{5.6b}$$

and the $c_j$ are arbitrary coefficients.

We substitute (5.6a) into (5.1a) and use (5.5) and $\lambda = O(\varepsilon^2)$. For $x$ near $x_j$, we get that $\phi_{1j}(y)$ satisfies

$$c_j L_\varepsilon \phi_{1j} \sim -\frac{q u_j^p h_{l_j}^q}{h_e^{q+1}}\left[c_j h_{ex}(x_j+\varepsilon y) - h_{l_j}^{\gamma}\eta_0(x_j+\varepsilon y)\right]\,. \tag{5.7}$$

Before solving this equation for $\phi_{1j}$ we need to determine an important continuity property of the right-hand side of (5.7).

Substituting (5.6a) into (5.1b), we get that $\eta_0$ satisfies

$$D\eta_{0xx} - \mu\eta_0 = -\varepsilon^{-2} m \frac{a_e^{m-1}}{h_e^s}\,(\phi_0 + \varepsilon\phi_1) + \varepsilon^{-1} s \frac{a_e^m}{h_e^{s+1}}\eta_0\,, \qquad -1 < x < 1\,. \tag{5.8}$$

Since $\phi_0$ is a linear combination of $u_j'$, it follows that the term multiplied by $\phi_0$ on the right-hand side in (5.8) behaves like a dipole. Hence, for $\varepsilon \ll 1$, this term is a linear combination of $\delta'(x - x_j)$ for $j = 1, .., k$, where $\delta(x)$ is the delta function. Thus, $\eta_0$ will be discontinuous across $x = x_j$. However, if we define the function $f(x)$ by

$$f(x) \equiv h_{l_j}^{\gamma}\eta_0(x) - c_j h_{ex}(x)\,, \tag{5.9}$$

then $f$ is continuous across $x = x_j$. To see this, we differentiate (1.1b) for $h_e$ with respect to $x$ and subtract appropriate multiples of the resulting equation and (5.8) to find that the dipole term cancels exactly. Thus, $f$ is continuous across $x = x_j$, and we have $\langle f\rangle_j = f(x_j)$. However, $\langle h_{ex}\rangle_j = 0$ from (5.3). Hence, $f(x_j) = h_{l_j}^{\gamma}\langle\eta_0\rangle_j$. Therefore, for $\varepsilon \ll 1$, we get from (5.7) that $\phi_{1j}$ satisfies

$$c_j L_\varepsilon \phi_{1j} \sim q u_j^p h_{l_j}^{\gamma-1}\langle\eta_0\rangle_j\,. \tag{5.10}$$

Since $L_\varepsilon u_j = (p-1)u_j^p + O(\varepsilon)$, (5.10) is easily solved to get

$$c_j\phi_{1j}(y) = \frac{q}{p-1}u_j(y)h_{l_j}^{\gamma-1}\langle\eta_0\rangle_j + O(\varepsilon)\,. \tag{5.11}$$

This condition shows that $\phi_{1j}$ is continuous across $x = x_j$ and has the form of a spike. This implies that the term in (5.8) proportional to $\phi_1$ behaves like a linear combination of $\delta(x - x_j)$ when $\varepsilon \ll 1$ and, most importantly, is *of the same order* in $\varepsilon$ as the dipole term proportional to $\phi_0$. This shows the fact that we need to determine the approximate eigenfunction for $\phi$ to both the $O(1)$ and $O(\varepsilon)$ terms in order to calculate an eigenvalue of order $O(\varepsilon^2)$.

Next, let $\varepsilon \to 0$ and use (5.6b) to calculate for $x$ near $x_j$ that

$$-\varepsilon^{-2} m \frac{a_e^{m-1}}{h_e^s}\phi_0 \sim -2c_j\sqrt{\mu D}\tanh(z_j)h_{l_j}^{1-\gamma}\,\delta'(x - x_j)\,, \tag{5.12a}$$

$$-\varepsilon^{-1} m \frac{a_e^{m-1}}{h_e^s}\phi_{1j} \sim -2c_j m\sqrt{\mu D}\tanh(z_j)h_{l_j}^{1-\gamma}\left(\frac{\int_{-\infty}^{\infty} u_c^{m-1}\phi_{1j}\,dy}{\int_{-\infty}^{\infty} u_c^m\,dy}\right)\delta(x - x_j)\,. \tag{5.12b}$$

Substituting (5.12) into (5.8), and using the formula (5.11) for $\phi_{1j}$, we get

$$D\eta_{0xx} - \left[\mu + 2s\sqrt{\mu D}\sum_{j=1}^{k}\tanh(z_j)\delta(x-x_j)\right]\eta = -2\sqrt{\mu D}\sum_{j=1}^{k} c_j \tanh(z_j) h_{l_j}^{1-\gamma}\delta'(x-x_j) - 2\sqrt{\mu D}\frac{qm}{p-1}\sum_{j=1}^{k}\tanh(z_j)\langle\eta_0\rangle_j\delta(x-x_j)\,. \tag{5.13}$$

This problem is equivalent to

$$D\eta_{0xx} - \mu\eta_0 = 0\,, \qquad -1 < x < 1\,; \qquad \eta_{0x}(\pm 1) = 0\,, \tag{5.14a}$$

$$[D\eta_0]_j = -2\sqrt{\mu D}c_j\tanh(z_j)h_{l_j}^{1-\gamma}\,; \qquad [D\eta_{0x}]_j = 2\sqrt{\mu D}\tilde{s}\tanh(z_j)\langle\eta_0\rangle_j\,, \tag{5.14b}$$

$$\tilde{s} \equiv s - \frac{qm}{p-1}\,. \tag{5.14c}$$

Next, we estimate the small eigenvalue. Substitute (5.6) into (5.1a) and multiply both sides of (5.1a) by $u_j'$. Integrating the resulting equation across the domain, we get

$$\sum_{i=1}^{k}\left(u_j', c_i L_\varepsilon u_i'\right) + \varepsilon\sum_{i=1}^{k}\left(u_j', c_i L_\varepsilon\phi_{1i}\right) - \varepsilon q\left(u_j', \frac{a_e^p\eta_0}{h_e^{q+1}}\right) \sim \lambda\sum_{i=1}^{k}\left(c_i u_i', u_j'\right)\,. \tag{5.15}$$

Here we have defined $(f,g) \equiv \int_{-1}^{1} f(x)g(x)\,dx$. To within negligible exponentially small terms, the dominant contribution in the sum comes from $i=j$ since $u_j'$ is exponentially localized near $x = x_j$. Thus, (5.15) becomes

$$c_j\left(u_j', L_\varepsilon u_j'\right) + \varepsilon c_j\left(u_j', L_\varepsilon\phi_{1j}\right) - \varepsilon q h_{l_j}^{q+\gamma}\left(u_j', \frac{u_j^p\eta_0}{h_e^{q+1}}\right) \sim \lambda c_j\left(u_j', u_j'\right)\,. \tag{5.16}$$

Since $L_\varepsilon$ is self-adjoint, we integrate by parts on the second term on the left-hand side of (5.16) and use (5.5) for $L_\varepsilon u_j'$. The integrands are localized near $x = x_j$. Thus, writing the resulting integrals in terms of the stretched variable $y = \varepsilon^{-1}(x - x_j)$, we get

$$\varepsilon^2 q c_j h_{l_j}^q\int_{-\infty}^{\infty}\frac{u_j^p u_j'}{h_e^{q+1}}h_{ex}\,dy - \varepsilon^2 q h_{l_j}^{q+\gamma}\int_{-\infty}^{\infty}\frac{u_j^p u_j'}{h_e^{q+1}}\eta_0\,dy + \varepsilon^3 q c_j h_{l_j}^q\int_{-\infty}^{\infty}\frac{u_j^p\phi_{1j}}{h_e^{q+1}}h_{ex}\,dy \sim \varepsilon\lambda c_j\int_{-\infty}^{\infty}\left(u_c'\right)^2\,dy\,. \tag{5.17}$$

In this expression $\eta_0 = \eta_0(x_j + \varepsilon y)$, $h_e = h_e(x_j + \varepsilon y)$, and $h_{ex} = h_{ex}(x_j + \varepsilon y)$.

We now estimate each of the terms in (5.17). Since $[\phi_{1j}]_j = 0$, $\langle h_{ex}\rangle_j = 0$, and $u_j'$ is odd, it follows that

$$\int_{-\infty}^{\infty} \frac{u_j^p \phi_{1j}}{h_e^{q+1}} h_{ex}\, dy = o(1) \qquad \text{as} \quad \varepsilon \to 0\,. \tag{5.18}$$

Hence, the third integral on the left-hand side of (5.17) will be $o(\varepsilon^3)$ and can be neglected. Next, we combine the first two terms on the left-hand side of (5.17) to get

$$\varepsilon^2 q c_j h_{l_j}^q \int_{-\infty}^{\infty} \frac{u_j^p u_j'}{h_e^{q+1}} h_{ex}\, dy - \varepsilon^2 q h_{l_j}^{q+\gamma} \int_{-\infty}^{\infty} \frac{u_j^p u_j'}{h_e^{q+1}} \eta_0\, dy = -\varepsilon^2 q h_{l_j}^q \int_{-\infty}^{\infty} \frac{u_j' u_j^p}{h_e^{q+1}} f(x_j + \varepsilon y)\, dy\,. \tag{5.19}$$

Here $f(x)$, defined in (5.9), is continuous across $x = x_j$ but its derivative is not. For $\varepsilon \ll 1$, we calculate

$$-\varepsilon^2 q h_{l_j}^q \int_{-\infty}^{\infty} \frac{u_j' u_j^p}{h_e^{q+1}} f(x_j + \varepsilon y)\, dy \sim \varepsilon^3 q \frac{c_j h_{exx}(x_j)}{h_{l_j}} \int_{-\infty}^{\infty} y u_j' u_j^p\, dy - \varepsilon^3 q h_{l_j}^{\gamma-1} \langle \eta_{0x}\rangle_j \int_{-\infty}^{\infty} y u_j' u_j^p\, dy\,. \tag{5.20}$$

Upon integrating by parts in (5.20), and using $h_{exx}(x_j) = \mu h_{l_j}/D$, we get

$$\varepsilon^2 q h_{l_j}^{1+q} \int_{-\infty}^{\infty} \frac{u_j' u_j^p}{h_e^{q+1}} \left( \frac{c_j h_{ex}}{h_{l_j}} - h_{l_j}^{\gamma-1} \eta_0 \right) dy \sim \frac{\varepsilon^3 q}{p+1} \left( h_{l_j}^{\gamma-1} \langle \eta_{0x}\rangle_j - \frac{c_j \mu}{D} \right) \int_{-\infty}^{\infty} [u_c(y)]^{p+1}\, dy\,. \tag{5.21}$$

Substituting (5.18) and (5.21) into (5.17), we obtain a formula for $\lambda$. We summarize the result (redefining $\eta_0$ for convenience) as follows:

**Proposition 5.1**: *The eigenvalues of order $O(\varepsilon^2)$ for (2.16) satisfy*

$$\lambda c_j \int_{-\infty}^{\infty} \left[u_c'(y)\right]^2 dy \sim \frac{\varepsilon^2 q}{p+1} \int_{-\infty}^{\infty} [u_c(y)]^{p+1}\, dy \left( h_{l_j}^{\gamma-1} \langle \eta_x\rangle_j - \frac{c_j \mu}{D} \right), \qquad j = 1, .., k\,. \tag{5.22}$$

*Here $\langle \eta_x\rangle_j$ is to be calculated from (5.14).*

## 5.2 Analyzing the Matrix Eigenvalue Problem

We now calculate $\langle \eta_x\rangle_j$ from the solution to (5.14). The solution to (5.14) can be decomposed as

$$\eta(x) = \sum_{j=1}^{k} \left( 2\sqrt{\mu D} \tanh(z_j) h_{l_j}^{1-\gamma} c_j g(x; x_j) + m_j G(x; x_j) \right), \tag{5.23}$$

for some coefficients $m_j$, for $j = 1, .., k$. Here $G$ satisfies (2.28), and $g(x; x_j)$ is the dipole Green's function satisfying

$$Dg_{xx} - \mu g = -\delta'(x - x_j)\,, \qquad -1 < x < 1\,, \tag{5.24a}$$

$$g_x(\pm 1; x_j) = 0\,. \tag{5.24b}$$

Satisfying the jump conditions in (5.14b), we get the following matrix problem for the coefficients $m_k$:

$$\left(I + \tilde{s}\sqrt{\mu D}\,\mathcal{C}\,\mathcal{G}\right)\boldsymbol{m} = -\tilde{s}(\mu D)\,\mathcal{C}\,\mathcal{P}_g\,\mathcal{C}\,\mathcal{H}^{1-\gamma}\boldsymbol{c}\,. \tag{5.25}$$

Here $\mathcal{G}$, $\mathcal{H}$, and $\mathcal{C}$ are defined in (3.9), (3.11), and (3.13), respectively. Also, $\mathcal{P}_g$, $\boldsymbol{c}$ and $\boldsymbol{m}$ are defined by

$$\mathcal{P}_g \equiv \begin{pmatrix} \langle g(x_1; x_1)\rangle_0 & \cdots & g(x_1; x_k) \\ \vdots & \ddots & \vdots \\ g(x_k; x_1) & \cdots & \langle g(x_k; x_k)\rangle_k \end{pmatrix}, \qquad \boldsymbol{m} \equiv \begin{pmatrix} m_1 \\ \vdots \\ m_k \end{pmatrix}, \qquad \boldsymbol{c} \equiv \begin{pmatrix} c_1 \\ \vdots \\ c_k \end{pmatrix}. \tag{5.26}$$

The problem (5.25) determines $\boldsymbol{m}$ in terms of $\boldsymbol{c}$. Then, using (5.26), we can calculate $\langle \eta_x\rangle_j$, for $j = 1, \ldots, k$, from the matrix problem

$$\langle \boldsymbol{\eta_x}\rangle = \sqrt{\mu D}\,\mathcal{G}_g\,\mathcal{C}\,\mathcal{H}^{1-\gamma}\boldsymbol{c} + \mathcal{P}\boldsymbol{m}\,, \tag{5.27}$$

where $\mathcal{G}_g$ is the Green's dipole matrix defined by

$$\mathcal{G}_g \equiv \begin{pmatrix} g_x(x_1; x_1) & \cdots & g_x(x_1; x_k) \\ \vdots & \ddots & \vdots \\ g_x(x_k; x_1) & \cdots & g_x(x_k; x_k) \end{pmatrix}, \tag{5.28}$$

and

$$\mathcal{P} \equiv \begin{pmatrix} \langle G_x(x_1; x_1)\rangle_0 & \cdots & G_x(x_1; x_k) \\ \vdots & \ddots & \vdots \\ G_x(x_k; x_1) & \cdots & \langle G_x(x_k; x_k)\rangle_k \end{pmatrix}, \qquad \langle \boldsymbol{\eta_x}\rangle \equiv \begin{pmatrix} \langle \eta_x\rangle_1 \\ \vdots \\ \langle \eta_x\rangle_k \end{pmatrix}. \tag{5.29}$$

Next, we define $\sigma$ by

$$\lambda = \frac{\varepsilon^2 q\sigma}{(p+1)}\left(\frac{\int_{-\infty}^{\infty}[u_c(y)]^{p+1}\,dy}{\int_{-\infty}^{\infty}[u_c'(y)]^2\,dy}\right). \tag{5.30}$$

Substituting (5.27) and (5.30) into (5.22), we get a matrix eigenvalue problem for $\sigma$ and $\boldsymbol{c}$

$$\sqrt{\mu D}\,\mathcal{H}^{\gamma-1}\,\mathcal{G}_g\,\mathcal{C}\,\mathcal{H}^{1-\gamma}\boldsymbol{c} + \mathcal{H}^{\gamma-1}\,\mathcal{P}\boldsymbol{m} = \left(\sigma + \frac{\mu}{D}\right)\boldsymbol{c}\,. \tag{5.31}$$

Here $\boldsymbol{m}$ is determined in terms of $\boldsymbol{c}$ by (5.25).

The next step in the analysis is to reduce (5.25) and (5.31) to an equivalent generalized eigenvalue problem. We begin by solving (5.25) for $\boldsymbol{m}$ by inverting the matrix on the left-hand side of (5.25). We calculate, using $\mathcal{G} = \mathcal{B}^{-1}/\sqrt{\mu D}$ from (3.22), that

$$\left(I + \tilde{s}\sqrt{\mu D}\,\mathcal{C}\,\mathcal{G}\right)^{-1} = \mathcal{B}\,\left(\mathcal{C}^{-1}\,\mathcal{B} + \tilde{s}I\right)^{-1}\,\mathcal{C}^{-1}\,. \tag{5.32}$$

From the assumption (1.2) on the exponents, we have $\tilde{s} < -1$. A sufficient condition for the matrix to be invertible is that $e_m + \tilde{s} < 0$, where $e_m$ is the maximum eigenvalue of the matrix $\tilde{\mathcal{E}} \equiv \mathcal{C}^{-1}\mathcal{B}$. By comparing with Corollary 3.2, and using the definition of $\tilde{s}$ in (5.14c), we see that this invertibility condition is precisely the condition that the asymmetric spike pattern is stable with respect to the large $O(1)$ eigenvalues. We will assume that this condition holds. The matrix $\tilde{\mathcal{E}}$ is decomposed as

$$\tilde{\mathcal{E}} \equiv \mathcal{C}^{-1}\mathcal{B} = Q\mathcal{K}Q^{-1}\,, \tag{5.33}$$

where $Q$ and $\mathcal{K}$ are the matrices of eigenvectors and eigenvalues of $\tilde{\mathcal{E}}$, respectively. Substituting (5.33) into (5.32), and solving for $\boldsymbol{m}$ in (5.25), we get

$$\boldsymbol{m} = -\tilde{s}(\mu D)\,\mathcal{B}\,Q\,\left(\mathcal{K} + \tilde{s}I\right)^{-1}\,Q^{-1}\,\mathcal{P}_g\,\mathcal{C}\,\mathcal{H}^{1-\gamma}\boldsymbol{c}\,. \tag{5.34}$$

Next, we substitute (5.34) into (5.31) to obtain

$$\mathcal{H}^{\gamma-1}\,\left[\sqrt{\mu D}\,\mathcal{G}_g\,\mathcal{C} - \tilde{s}(\mu D)\,\mathcal{P}\,\mathcal{B}\,Q\,\left(\mathcal{K} + \tilde{s}I\right)^{-1}\,Q^{-1}\,\mathcal{P}_g\,\mathcal{C}\right]\,\mathcal{H}^{1-\gamma}\boldsymbol{c} = \left(\sigma + \frac{\mu}{D}\right)\boldsymbol{c}\,. \tag{5.35}$$

In Appendix A, we show that

$$\mathcal{G}_g = \frac{\sqrt{\mu}}{D^{3/2}}\mathcal{B}_g^{-1}\,, \tag{5.36}$$

where $\mathcal{B}_g$ is a tridiagonal matrix. The matrix $\mathcal{B}_g$ has exactly the same form as given in (3.23a), except that now the definitions of the coefficients in (3.23b) are to be replaced with

$$c_1 = \coth(z_1 + z_2) + \coth z_1\,; \qquad c_k = \coth(z_k + z_{k-1}) + \coth z_k\,, \tag{5.37a}$$

$$c_j = \coth(z_{j+1} + z_j) + \coth(z_j + z_{j-1})\,, \quad j = 2, .., k-1\,; \quad d_j = -\mathrm{csch}(z_j + z_{j+1})\,, \quad j = 1, .., k-1\,. \tag{5.37b}$$

Here $z_j$ is defined in (3.13). Substituting (5.36) into (5.35), we obtain

$$\mathcal{H}^{\gamma-1}\,\left[\mathcal{B}_g^{-1}\,\mathcal{C}-\mathcal{P}\,\mathcal{B}\,Q\,\mathcal{D}\,Q^{-1}\,\mathcal{P}_g\,\mathcal{C}\right]\,\mathcal{H}^{1-\gamma}\boldsymbol{c}=\left(\frac{\sigma D}{\mu}+1\right)\boldsymbol{c}\,, \tag{5.38}$$

where $\mathcal{D}$ is the diagonal matrix defined by

$$\mathcal{D}\equiv\tilde{s}D^2\,(\mathcal{K}+\tilde{s}I)^{-1}\ . \tag{5.39}$$

Since $\tilde{s}<-1$ and $\mathcal{K}+\tilde{s}I<0$, we conclude that $\mathcal{D}$ is a positive diagonal matrix.

Finally, we introduce $\boldsymbol{u}$ defined by

$$\boldsymbol{u}=\mathcal{B}_g^{-1}\,\mathcal{C}\,\mathcal{H}^{1-\gamma}\,\boldsymbol{c}\,. \tag{5.40}$$

Substituting (5.40) into (5.38), and using (5.30), we obtain the following main result:

**Proposition 5.2**: *For $\varepsilon\ll 1$, the eigenvalues of (3.2) of order $\lambda=O(\varepsilon^2)$ satisfy*

$$\lambda_j\sim\frac{\varepsilon^2 q\mu}{D(p+1)}\left(\frac{\int_{-\infty}^{\infty}[u_c(y)]^{p+1}\,dy}{\int_{-\infty}^{\infty}[u_c'(y)]^2\,dy}\right)\left(\frac{1}{\omega_j}-1\right)\,,\qquad j=1,..,k\,, \tag{5.41}$$

*where $\omega_j$ is an eigenvalue of the generalized eigenvalue problem*

$$\mathcal{C}^{-1}\mathcal{B}_g\boldsymbol{u}=\omega\,(I+\mathcal{R})\,\boldsymbol{u}\,. \tag{5.42a}$$

*Here $\mathcal{R}$ is given by*

$$\mathcal{R}\equiv-\mathcal{P}\,\mathcal{B}\,Q\,\mathcal{D}\,Q^{-1}\,\mathcal{P}_g\,\mathcal{B}_g\,. \tag{5.42b}$$

*The eigenvector $\phi$ is given by (5.6), where*

$$\boldsymbol{c}_j=\mathcal{H}^{\gamma-1}\,\mathcal{C}^{-1}\,\mathcal{B}_g\boldsymbol{u}_j\,, \tag{5.43}$$

*and $\boldsymbol{u}_j$ is an eigenvector of (5.42). The matrix products $\mathcal{PB}$ and $\mathcal{P}_g\mathcal{B}_g$ are tridiagonal and they are given explicitly in (A.7) and (A.13) of Appendix A, respectively.*

For a symmetric $k$-spike pattern, $\omega_j$ can be calculated analytically from (5.42), since it this case $\mathcal{C}$ is a constant multiple of the identity matrix and $\mathcal{B}_g$ and $\mathcal{R}$ were found to have exactly the same eigenspace. This analysis was done in §4.2 of [5], and the following result was given in Proposition 11 of [5].

**Proposition 5.3** (**From [5]**): *Consider a symmetric k-spike equilibrium solution where* $z_1 = z_2 = , .., = z_k = z_c$. *Then, for* $\varepsilon \ll 1$, *the eigenvalues* $\lambda$ *of (3.2) of order* $O(\varepsilon^2)$ *are all real, and they are negative when*

$$D < D_m = \frac{\mu}{k^2 z_c^2}\,, \tag{5.44}$$

*where* $z_c$ *is given in (2.14). When* $D > D_m$, *then* $k-1$ *small eigenvalues are positive. When* $D = D_m$, $\lambda = 0$ *is a small eigenvalue of algebraic multiplicity* $k-1$. *Furthermore,* $D_m < D_k$, *where* $D_k$, *given in (4.15) is the largest value of* $D$ *for which the symmetric branch* $s_k$ *is stable with respect to the large* $O(1)$ *eigenvalues.*

Hence, the symmetric branch is stable with respect to *both* the small and large eigenvalues when $D < D_m$. Qualitatively, this implies that as $D$ is decreased below the bifurcation point $D = D_m$, where asymmetric solution branches emerge from the symmetric branch $s_k$, the symmetric branch becomes stable with respect to the small eigenvalues. The final question we address is to determine the stability with respect to the small eigenvalues of the $k-1$ asymmetric branches (ignoring in the counting the different possible orientations of the small and large spikes) that emerge from $s_k$ and that provide connections to the other symmetric branches $s_j$ for $j = 1, .., k-1$. This stability calculation using (5.42) must be done numerically.

The numerical procedure is as follows. Fix $k_1$, $k_2$, $\mu$, $\tilde{s}$, $r$, and a specific orientation of the large and small spikes. Let $D$ be the parameter. Compute $z$ and $\tilde{z}$ from (2.19) and determine $z_1$,..,$z_k$. Then, calculate $\mathcal{PB}$ and $\mathcal{P}_g\mathcal{B}_g$ from (A.7) and (A.13), respectively. The eigenvectors and eigenvalues of $\mathcal{C}^{-1}\mathcal{B}$ are computed numerically using LAPACK [1] to obtain $\mathcal{Q}$, $\mathcal{K}$, and $\mathcal{D}$. Finally, we use a generalized eigenvalue problem solver from LAPACK to calculate the eigenvalues $\omega_j$ from (5.42). When $D = D_m$, $\lambda_j = 0$ has multiplicity $k-1$, and hence $\omega_j = 1$ for $j = 1, .., k-1$ at this value of $D$. We define $\omega^*$ by

$$\omega^* = \mathrm{Min}(\omega_j) \qquad \text{such that} \quad \omega_j > 0 \qquad \text{for} \quad j = 1, .., k\,. \tag{5.45}$$

Clearly, $\omega^*$ is defined for $D$ near $D_m$. From Proposition 5.2, we conclude that a $k$-spike pattern is unstable when $\omega^* < 1$.

For each specific spike pattern shown in §4, we have computed $\omega^*$ as a function of $D$ over the range of values of $D$ for which the specific exists and is stable with respect to the large $O(1)$ eigenvalues. In each case, we have found that $\omega^* < 1$ over this range of $D$, and so all of the asymmetric bifurcating branches computed in §4 are *unstable* with respect to the small eigenvalues. To illustrate our results, in Fig. 14 we plot $\omega^*$ versus $D$ for the AB patterns of Result 4.1 for both

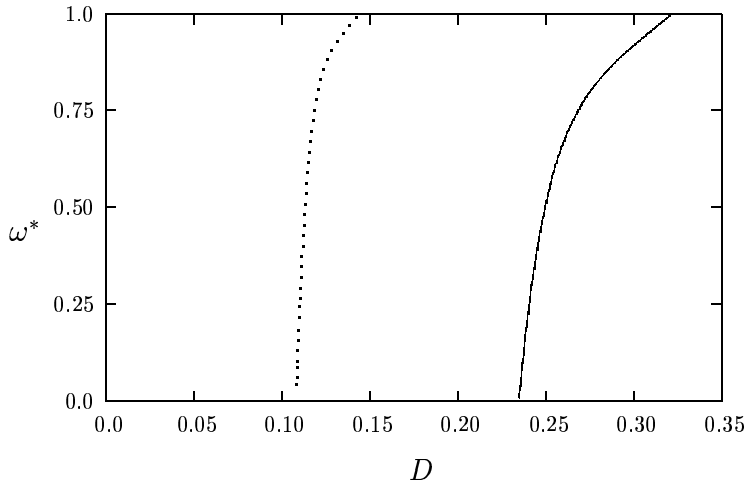


Figure 14: Plot of $\omega^*$, defined in (5.45), versus $D$ for a two-spike pattern of the type AB. The solid and dotted curves are for the parameter sets $(p, q, m, s) = (2, 1, 2, 0)$ and $(p, q, m, s) = (4, 2, 2, 0)$, respectively. Here $\mu = 1$.

$r = 1$ and $r = 3$. Similar plots are shown in Fig. 15(a) and Fig. 15(b) for the ABB and ABBB patterns, respectively. Notice, from these figures that as $D$ approaches the value for which the asymmetric branch bifurcates from the symmetric branch, we have $\omega^* \to 1$. Alternatively, since $\mathcal{R}$ in (5.42b) becomes unbounded as $D$ approaches $D_e$ from above, where $D_e$ was the critical stability value for the large eigenvalues, we would expect that $\omega^* \to 0$ as $D \to D_e$. This is exactly the behavior that is observed in these figures. Although we do not have an analytical proof in general that the bifurcating asymmetric branches are always unstable with respect to the small eigenvalues, this appears to be true based on our numerical evidence.

# 6 Conclusions

We have used formal asymptotic analysis to construct asymmetric equilibrium spike patterns for a simplified form of the Gierer-Meinhardt model. We have also analyzed the linear stability properties of these solutions. We have found that there are ranges of $D$ for which these asymmetric solutions are stable with respect to the large $O(1)$ eigenvalues. However, based on numerical evidence, these solutions are always unstable with respect to the small $O(\varepsilon^2)$ eigenvalues. As extensions to this work, a rigorous framework for the analysis of symmetric and asymmetric spike solutions is given

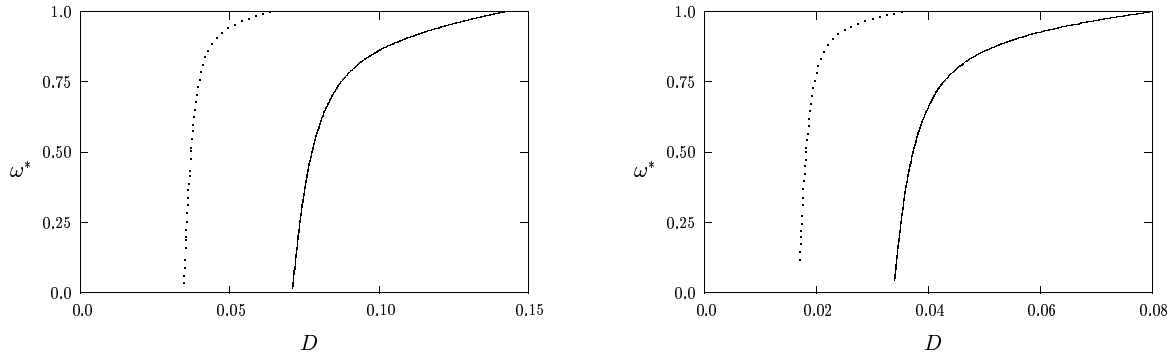


(a) ABB pattern

(b) ABBB pattern

Figure 15: Plot of $\omega^*$, defined in (5.45), versus $D$ for three-spike and four-spike patterns of the type ABB and ABBB. The solid and dotted curves are for the parameter sets $(p,q,m,s) = (2,1,2,0)$ and $(p,q,m,s) = (4,2,2,0)$, respectively. Here $\mu = 1$.

in [15]. The dynamics of spike solutions for (1.1) is studied in [7] using asymptotic and numerical methods.

The analysis presented above generalizes the typical Turing analysis based on linearizing a reaction-diffusion equation around a spatially homogeneous equilibrium state. It would be interesting to see if similar methods to those used here could be employed to analyze the existence and stability of symmetric and asymmetric equilibrium spike patterns for other problems, including related one-dimensional reaction-diffusion systems and for the Gierer-Meinhardt model in a multi-dimensional setting.

# A Calculation of the Matrices $\mathcal{B}$, $\mathcal{B}_g$, $\mathcal{P}\mathcal{B}$, and $\mathcal{P}_g\mathcal{B}_g$

Consider the boundary value problem

$$Dy'' - \mu y = 0\,, \qquad y'(\pm 1) = 0\,, \tag{A.1a}$$

$$[y]_j = 0\,, \qquad \left[Dy'\right]_j = -\omega_j\,, \tag{A.1b}$$

for $j = 1, \ldots, k$, where $[v]_j \equiv v(x_{j+}) - v(x_{j-})$ and $x_j$ satisfies (2.29). The solution is

$$y(x) = \sum_{j=1}^{k} G(x; x_j)\omega_j \,, \tag{A.2}$$

where $G$ satisfies (2.28). Define the $k$-vectors $\boldsymbol{y}$ and $\langle \boldsymbol{y}' \rangle$ by

$$\boldsymbol{y}^t = (y_1, \ldots, y_k) \,, \qquad \langle \boldsymbol{y}' \rangle^t = \Big( \langle y' \rangle_1, \ldots, \langle y' \rangle_k \Big) \,, \tag{A.3}$$

where $y_j \equiv y(x_j)$ and $\langle y' \rangle_j \equiv \Big( y'(x_{j+}) + y'(x_{j-}) \Big)/2$. Then, we obtain from (A.2) that

$$\boldsymbol{y} = \mathcal{G}\boldsymbol{\omega} \,, \qquad \langle \boldsymbol{y}' \rangle = \mathcal{P}\boldsymbol{\omega} \,, \qquad \rightarrow \qquad \langle \boldsymbol{y}' \rangle = \mathcal{P}\mathcal{G}^{-1}\boldsymbol{y} \,, \tag{A.4}$$

where $\boldsymbol{\omega}^t = (\omega_1, \ldots, \omega_k)$. Here the matrices $\mathcal{G}$ and $\mathcal{P}$ are defined in (3.9) and (5.29), respectively. To determine these matrices explicitly we solve (A.1) analytically on each subinterval and impose the continuity of $y$ to get

$$y(x) = \begin{cases} y_1 \frac{\cosh[\zeta(1+x)]}{\cosh[\zeta(1+x_1)]} \,, & -1 < x < x_1 \,, \\ y_j \frac{\sinh[\zeta(x_{j+1}-x)]}{\sinh[\zeta(x_{j+1}-x_j)]} + y_{j+1} \frac{\sinh[\zeta(x-x_j)]}{\sinh[\zeta(x_{j+1}-x_j)]} \,, & x_j < x < x_{j+1} \,, \quad j = 1, \ldots, k-1 \,, \\ y_k \frac{\cosh[\zeta(1-x)]}{\cosh[\zeta(1-x_k)]} \,, & x_k < x < 1 \,, \end{cases} \tag{A.5}$$

where $\zeta \equiv \sqrt{\mu/D}$. Imposing the condition $[Dy']_j = -\omega_j$, and using (2.29) for $x_j$, we can obtain from (A.5) and (A.4) that

$$\mathcal{B}\boldsymbol{y} = \frac{1}{\sqrt{\mu D}}\boldsymbol{\omega} \,, \qquad \rightarrow \qquad \mathcal{G} = \frac{1}{\sqrt{\mu D}}\mathcal{B}^{-1} \,, \tag{A.6}$$

where $\mathcal{B}$ is defined in (3.23). Next, we use (A.4) and (A.6) to get $\langle \boldsymbol{y}' \rangle = \sqrt{\mu D}\mathcal{P}\mathcal{B}\boldsymbol{y}$. By calculating $\langle \boldsymbol{y}' \rangle$ in terms of $\boldsymbol{y}$ from (A.5), we get a formula for $\mathcal{P}\mathcal{B}$

$$\mathcal{P}\mathcal{B} \equiv \frac{1}{2D} \begin{pmatrix} c_1 & d_1 & 0 & \cdots & 0 & 0 & 0 \\ -d_1 & c_2 & \ddots & \ddots & \ddots & 0 & 0 \\ 0 & \ddots & \ddots & \ddots & \ddots & \ddots & 0 \\ \vdots & \ddots & \ddots & \ddots & \ddots & \ddots & \vdots \\ 0 & \ddots & \ddots & \ddots & \ddots & \ddots & 0 \\ 0 & 0 & \ddots & \ddots & \ddots & c_{k-1} & d_{k-1} \\ 0 & 0 & 0 & \cdots & 0 & -d_{k-1} & c_k \end{pmatrix} \,, \tag{A.7a}$$

with matrix entries defined by

$$c_1 = \tanh z_1 - \coth(z_1 + z_2)\,; \qquad c_k = \coth(z_k + z_{k-1}) - \tanh z_k\,, \tag{A.7b}$$

$$c_j = \coth(z_j + z_{j-1}) - \coth(z_j + z_{j+1})\,, \quad j = 2, .., k-1\,; \quad d_j = \operatorname{csch}(z_j + z_{j+1})\,, \quad j = 1, .., k-1\,. \tag{A.7c}$$

Here $z_j$ is defined in (3.13).

To calculate $\mathcal{B}_g$ and $\mathcal{P}_g\mathcal{B}_g$, we consider the related boundary value problem

$$Dy'' - \mu y = 0\,, \qquad y'(\pm 1) = 0\,, \tag{A.8a}$$

$$[Dy]_j = -\omega_j\,, \qquad \Big[y'\Big]_j = 0\,, \tag{A.8b}$$

for $j = 1, \ldots, k$. The solution is

$$y(x) = \sum_{j=1}^{k} g(x; x_k)\omega_k\,, \tag{A.9}$$

where $g$ satisfies (5.24). In terms of the matrices $\mathcal{G}_g$ and $\mathcal{P}_g$, defined in (5.28) and (5.26), respectively, we have that

$$\boldsymbol{y}' = \mathcal{G}_g\boldsymbol{\omega}\,, \qquad \langle \boldsymbol{y} \rangle = \mathcal{P}_g\boldsymbol{\omega}\,, \qquad \rightarrow \qquad \langle \boldsymbol{y} \rangle = \mathcal{P}_g\mathcal{G}_g^{-1}\boldsymbol{y}'\,, \tag{A.10}$$

where $\boldsymbol{\omega}^t = (\omega_1, \ldots, \omega_k)$. To determine $\mathcal{G}_g$ explicitly, we solve (A.8) analytically on each subinterval and impose the continuity of $y'$ to get

$$y(x) = \begin{cases} \frac{y_1'}{\zeta}\frac{\cosh[\zeta(1+x)]}{\sinh[\zeta(1+x_0)]}\,, & -1 < x < x_1\,, \\ \frac{y_{j+1}'}{\zeta}\frac{\cosh[\zeta(x-x_j)]}{\sinh[\zeta(x_{j+1}-x_j)]} - \frac{y_j'}{\zeta}\frac{\cosh[\zeta(x_{j+1}-x)]}{\sinh[\zeta(x_{j+1}-x_j)]}\,, & x_j < x < x_{j+1}\,, \quad j = 1, \ldots, k-1\,, \\ -\frac{y_k'}{\zeta}\frac{\cosh[\zeta(1-x)]}{\sinh[\zeta(1-x_k)]}\,, & x_k < x < 1\,, \end{cases} \tag{A.11}$$

where $\zeta = (\mu/D)^{1/2}$. We then impose the jump condition $[Dy]_j = -\omega_j$ to obtain

$$\mathcal{B}_g\boldsymbol{y}' = \frac{\sqrt{\mu}}{D^{3/2}}\boldsymbol{\omega}\,, \qquad \rightarrow \qquad \mathcal{G}_g = \frac{\sqrt{\mu}}{D^{3/2}}\mathcal{B}_g^{-1}\,, \tag{A.12}$$

where $\mathcal{B}_g$ has the tridiagonal form given in (3.23a) with matrix entries defined in (5.37). Finally, we use (A.10) and (A.12) to get $\langle \boldsymbol{y} \rangle = \mu^{-1/2}D^{3/2}\mathcal{P}_g\mathcal{B}_g\boldsymbol{y}'$. By calculating $\langle \boldsymbol{y} \rangle$ in terms of $\boldsymbol{y}'$ from

(A.11) we get a formula for $\mathcal{P}_g\mathcal{B}_g$

$$\mathcal{P}_g\mathcal{B}_g \equiv \frac{1}{2D}\begin{pmatrix} \tilde{c}_1 & d_1 & 0 & \cdots & 0 & 0 & 0 \\ -d_1 & c_2 & \ddots & \ddots & \ddots & 0 & 0 \\ 0 & \ddots & \ddots & \ddots & \ddots & \ddots & 0 \\ \vdots & \ddots & \ddots & \ddots & \ddots & \ddots & \vdots \\ 0 & \ddots & \ddots & \ddots & \ddots & \ddots & 0 \\ 0 & 0 & \ddots & \ddots & \ddots & c_{k-1} & d_{k-1} \\ 0 & 0 & 0 & \cdots & 0 & -d_{k-1} & \tilde{c}_k \end{pmatrix}, \tag{A.13a}$$

with (A.7c) still holds for $c_j$ and $d_j$, but (A.7b) is replaced by

$$\tilde{c}_1 = \coth z_1 - \coth(z_1 + z_2)\,; \qquad \tilde{c}_k = \coth(z_k + z_{k-1}) - \coth z_k\,, \tag{A.13b}$$

Hence the matrix products $\mathcal{P}\mathcal{B}$ and $\mathcal{P}_g\mathcal{B}_g$ are the same, except for different entries in the $(1,1)$ and $(k,k)$ positions.

## Acknowledgements

We are very grateful to Prof. A. Doelman of U. Amsterdam who suggested to us that asymmetric spike patterns should exist for the GM model. M. J. W. would like to thank the hospitality of Roderick Wong and the support of the Mathematics Department at the City University of Hong Kong, where this paper was written. J. W. thanks the support of RGC of Hong Kong.

## References

[1] E. Anderson et al. *Lapack User's Guide: Third Edition*, SIAM Publications (1999).

[2] A. Doelman, private communication.

[3] A. Gierer, H. Meinhardt, *A Theory of Biological Pattern Formation*, Kybernetik, **12**, (1972), pp. 30–39.

[4] L. Harrison, D. Holloway, *Order and Localization in Reaction-Diffusion Pattern*, Physica A, **222**, (1995), pp. 210-233.

[5] D. Iron, M. J. Ward, J. Wei, *The Stability of Spike Solutions to the One-Dimensional Gierer-Meinhardt Model*, submitted, Physica D, Jan. 2000.

[6] D. Iron, M. J. Ward, *A Metastable Spike Solution for a Non-Local Reaction-Diffusion Model*, SIAM J. Appl. Math., to appear, (2000).

[7] D. Iron, M. J. Ward, *The Dynamics of Multi-Spike Solutions to the One-Dimensional Gierer-Meinhardt Model*, preprint.

[8] H. Meinhardt, *Models of Biological Pattern Formation*, Academic Press, London (1982).

[9] W. Ni, *Diffusion, Cross-Diffusion, and their Spike-Layer Steady-States*, Notices of the AMS, Vol. **45**, No. 1, (1998), pp. 9-18.

[10] Y. Nishiura, *Coexistence of Infinitely Many Stable Solutions to Reaction-Diffusion Equations in the Singular Limit*, in Dynamics Reported: Expositions in Dynamical Systems Volume 3 (editors: C. K. R. T. Jones, U. Kirchgraber), Springer-Verlag, New York, (1995).

[11] I. Takagi, *Point-Condensation for a Reaction-Diffusion System*, J. Diff. Eq., **61**, (1986), pp. 208-249.

[12] A. Turing, *The Chemical Basis of Morphogenesis*, Phil. Trans. Roy. Soc. B, **327**, (1952), pp. 37-72.

[13] J. Wei, *On Single Interior Spike Solutions for the Gierer-Meinhardt System: Uniqueness and Stability Estimates*, Europ. J. Appl. Math., Vol. **10**, No. 4, (1999), pp. 353-378.

[14] J. Wei, *Point–Condensations Generated by the Gierer-Meinhardt System: a Brief Survey*, book chapter in "New Trends in Nonlinear Partial Differential Equations 2000", (Y. Morita, H. Ninomiya, E. Yanagida, and S. Yotsutani editors), pp. 46-59.

[15] J. Wei, M. Winter, *The Gierer-Meinhardt System: Existence and Stability of N-Peaked Solutions*, preprint.